# Section on Functional Imaging Methods (2021-2024)

**Peter A. Bandettini, Ph.D.**
**Report for the Board of Scientific Counselors Review**

## Table of Contents

# Executive Summary

For the past 25 years, the research of the Section on Functional Imaging Methods (SFIM) has aimed to advance the utility of fMRI both towards understanding the functional organization of the human brain and for increased clinical utility. The key challenges involve imaging faster, with greater brain coverage, at higher resolution, and with more sensitivity and specificity to neuronal activity or cerebral hemodynamic/neurofluid physiology. Advancement of fMRI can be understood as organized across four domains: Hardware and Pulse sequences, Signal Interpretation, Paradigm Designs and Processing Methods, and finally, Applications. Our group has developed novel high-resolution pulse sequences that are sensitive to blood volume changes which are more localized to the sources of neuronal activity. We have shed light on the temporal characteristics and neuronal correlates of resting state fluctuations. We have developed processing methods that allow precise characterization of specific spontaneous fluctuation dynamics and reduce dimensionality while minimizing information loss. We have also advanced naturalistic stimuli and intersubject correlation methods to derive insight into the neural correlates of individual traits and states. Finally, regarding applications, we have applied simultaneous multi-modal acquisition of pupillometry to capture and localize changes in attention and simultaneous EEG and eye tracking data to capture and localize fMRI signatures of arousal.

An advance in one domain leverages advances in other domains. For instance, pulse sequence advances in speed, resolution, or specificity allow more nuanced questions about the nature of the signal, which lead to novel applications. New insight into the temporal and spatial characteristics of the signal and noise allow for added prior knowledge to be used in processing methods, thus catalyzing more effective tools that provide insight into spatial and temporal characteristics of neuronal activity. Research that is positioned at the interface of the latest advances in these domains adds insight into the fMRI signal and noise, sheds light on the spatial and temporal features of brain function and provides information on the utility and robustness of the processing methods and pulse sequences themselves. The highest impact fMRI research straddles and integrates these domains.

SFIM has continuously positioned its research at the nexus of these four domains. We have identified gaps in fMRI capabilities and have sought to bridge these gaps through the development of novel pulse sequences, paradigms, processing methods that leverage what we understand about the spatial and temporal properties of the fMRI contrast and noise. Resultingly, we gain insight into the neuronal and physiologic underpinnings of the signal that then may iteratively be employed for subsequent methods development or to address neuroscience or clinical questions. Our group has thrived with a multi-disciplinary approach and a staff of individuals with highly diverse skills – all working together to advance fMRI spatial and temporal resolution, interpretability, replicability, and utility.

Since the last review, our research has focused on four areas where advancement in fMRI has the highest potential impact. These are: fMRI signal fluctuations and connectivity, ultra-high resolution or layer fMRI, multi-modal integration towards relating fMRI to underlying neuronal activity, and fMRI pulse sequence development.

# Significance

Functional MRI has unknowns and challenges that present barriers to its utility. The challenges that SFIM has addressed in the past four years include: 1. Performance of whole-brain fMRI at sub-millimeter resolution using a functional contrast that is localized to small regions of activation and sufficient sensitivity to deliver interpretable results in a single scanning session. 2. Development of methods for understanding and utilizing the temporal and spatial features of the spontaneous and task-related fMRI signal to fully differentiate neuronal activity from non-neuronal fluctuations, and to allow individual neural correlates to specific traits. 3. Integration of simultaneous physiological or performance measures to guide interpretation of the fMRI signal changes as they relate to attention, arousal, and behavior. 4. Develop functional MRI pulse sequences to measure and map novel physiologic information in the brain. All of these directions of SFIM are fundamentally important to fMRI as enhancement of its resolution, sensitivity, specificity, and robustness leads directly to enhanced utility in basic neuroscience research and clinical practice.

The ability to map **layer-specific neuronal activity** using **high-resolution fMRI** across the entire brain hypothetically allows derivation of cortical feedforward and feedback activity within and across regions, enabling the mapping of directional interaction and regional hierarchy – thus more deeply informing computational models. The challenges inherent to layer fMRI are many. Here we have advanced and refined whole-brain layer fMRI acquisition and processing strategies to improve time efficiency while reducing artifact and distortion, developed an approach for precise high-resolution functional registration, and have begun testing our approaches with applications related to the functional organization of layers. We also have continued to develop tools for time series analysis of layer-specific activity.

While **spontaneous resting state fluctuations** have been characterized by their spatial correlation structure and low frequency spectral density, their full complexity and information content has not yet been fully determined. Brief punctate correlated activity appears to drive specific functional network correlations, and lower temporal/spatial frequency waves may be more informative of arousal or other homeostatic processes. Here, we developed and compared methods for extraction of information from the resting state signal, including dimensionality reduction approaches and "edge" analyses that consider moment to moment correlations. Capturing and leveraging relevant **neuronal activation-related fluctuations** associated with naturalistic stimuli or tasks has been an area of intense research for over a decade. We have developed a naturalistic language assessment paradigm and demonstrated that, when comparing time-locked activity across pairs of subjects performing this task, we are able to differentiate the better readers from the poorer readers as well as identify previously missed prefrontal activity that may be fundamentally associated with these differences.

Integration of **multi-modal data**, including EEG, eye-tracking, and other measures more fully into the collection and analysis pipeline promises to enhance and guide the interpretation of fMRI data. Here we have implemented several human multi-modal measures to guide interpretation of arousal, conscious awareness, attention, ongoing physiologic processes, and in-scanner mental state. We have also collaborated with the Hillman group at Columbia University in a study comparing simultaneous wide-field Ca+ measures and blood oxygenation during different states of arousal and activity in a mouse model, comparing the spatial and temporal information content across both measures – revealing a clear temporal and spatial correlation between neuronal activity and hemodynamics. Lastly, we have used detailed post scan survey information to investigate the neuronal correlates of predominant in-scanner thoughts and wakefulness. We have started to explore the rich landscape of peripheral time series measures of Photoplesmography based blood oxygenation, volume, and pressure to determine the relationships between these measures and the resting state brain fMRI and CSF dynamics. .

We have also developed high resolution **pulse sequences** that though k-space registration and sorting to align with specific neuronal or physiologic events, can enhance image quality and temporal resolution. We have developed a high resolution pulse sequences that target CSF volume as a contrast as there is growing evidence that the dynamics of CSF volume and flow is highly sensitive to physiologic state and may provide insight into the glymphatic system and predict mental health pathology.

## Innovation and Appropriateness to the Intramural Environment

The research performed by SFIM integrates acquisition, paradigm, and processing methods; research in understanding the signal; and applications. Its suitability for the intramural environment is based on the requirement for uninterrupted access to substantial physical and human resources, extensive data analysis expertise, and intramural collaborations. Collaboration with fellow IRP PIs, Cores and Teams has been critical for the motivation and refinement of methods for deriving new information from the time series.

The typical projects of SFIM either require high stability over durations longer than most extramural funding periods, or are short term, iterative, and by necessity – exploratory and potentially high risk. Our focus of methods development does not fit within typical extramural funding categories. The NIMH Intramural Program support allows for a research approach that is optimal for our group: a focus on long-term goals, both high and low risk, as well as the flexibility to rapidly iterate, change direction, and explore when needed so that ideas may be rapidly tested.

# Background and Progress

## Theme 1: Layer fMRI

### 1.1 Whole-Brain Layer Connectivity Mapping with 3D VAPER fMRI

*Chai, Y.; Morgan, A. T.; Xie, H.; Li, L.; Huber, L.; Bandettini, P. A.; Sutton, B. P. Unlocking Near-Whole Brain, Layer-Specific Functional Connectivity with 3D VAPER fMRI. Imaging Neuroscience 2024.*

This study shows an new processing approach to leverage group data with layer-specific 3D VAPER (Integrated VAso and PERfusion contrast) imaging[1] in humans at 7 T with fMRI with 0.8 $mm^3$ voxel dimensions. This sequence has high sensitivity, specificity, and sensitivity to localized capillary changes due to the combination of both perfusion and blood volume contrast. It also benefits from direct registration to simultaneously collected, distortion-matched, and high structural contrast magnetization-transfer (MT) weighted structural images, and near-whole-brain coverage. To demonstrate effectiveness of 3D VAPER, we acquire fMRI data during both resting-state and movie-watching. Using a novel laminar-specific surface projection and multisubject averaging approach, layer-sensitive functional connectivity analysis pipeline, we mapped the distribution of laminar activation profiles within and across functional networks.

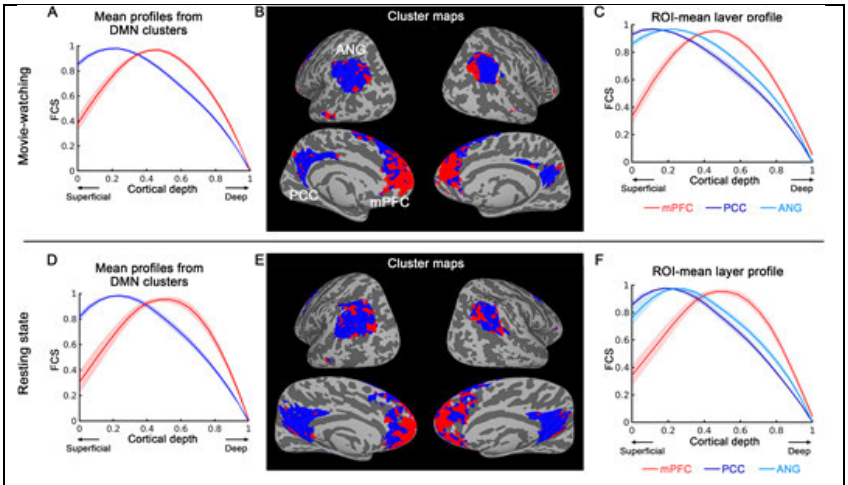


**Figure 1.** Laminar profile-based parcellation of default mode network (DMN) using k-means clustering at the group level (N = 24 for movie-watching and N = 12 for resting state). The DMN network region was individually defined using ICA and then averaged at group level. k = 2 was employed, and the mean functional connectivity strength (FCS) for each cluster was plotted as a function of cortical depth, as shown in (A) and (D). In (B) and (E), red regions represent FCS peaking at middle cortical depths, while the blue regions indicate FCS peaking at superficial cortical depths. (C) and (F) depict the mean laminar profiles of FCS within three main nodes of the DMN. The medial prefrontal cortex (mPFC) shows feedforward-driven connectivity, with FCS peaking at middle cortical depths. Conversely, the input to angular gyrus (ANG) and posterior cingulate (PCC) are predominantly feedback-driven, with FCS peaking at superficial cortical depths.

We used a segmented 3D-EPI with shot-selective controlled aliasing in parallel imaging (shot-selective CAIPI) sampling strategy as the acquisition for both functional VAPER and anatomical magnetization transfer (MT) imaging. MT has been shown to enhance structural contrast[2]. Within each selected network, we applied k-means clustering to group areas according to the similarity of their functional connectivity strength (FCS) across 18 cortical depths. We first input vertex-wise FCS laminar profiles in each network to the k-means clustering algorithm. This algorithm sorts network areas into two groups based purely on their cortical laminar profiles by maximizing within-cluster similarity and between-cluster dissimilarity, using correlation as a distance measure. This analysis was conducted on the group-averaged FCS map for each network.

Our results were able to differentiate layer-specific connectivity patterns within and across the default mode, somatomotor, and visual networks. Figure 1 demonstrates layer-based parcellation of the default mode network (DMN). Within the DMN, we identified two distinct types of connectivity based on the laminar feature: feedback and feedforward. The mPFC, a key hub within the DMN, predominantly displayed a feedforward-driven pattern with a connectivity strength peak at middle cortical depths. Conversely, the input to the PCC and ANG demonstrated primarily feedback-driven connectivity with FCS peaking at superficial cortical depths. Existing research on the DMN using dynamic causal modeling has found that the PCC sends out a driving input signal, while the mPFC plays

a regulatory role on the DMN network. This aligns with our findings that suggest the mPFC provides feedback to, and receives feedforward input from, other DMN nodes. In contrast, PCC and ANG send feedforward input to mPFC and receive feedback from mPFC.

Group level averaging at the layer level has been thought to be an intractable problem due to individual differences at the scale of a millimeter. Until now, layer-specific fMRI research has merely compared or averaged the 1D laminar profile plots across subjects. Our study overcomes those obstacles by introducing a cortical depth-specific surface registration method. This approach resolves this inherent challenge accurate data analysis and interpretation. For the first time, we have constructed a group-level brain map of fMRI connectivity layer patterns.

### 1.2 Layer-specific activation in human S1 during temporal prediction error processing

*Yu, Y.; Huber, L.; Yang, J.; Fukunaga, M.; Chai, Y.; Jangraw, D. C.; Chen, G.; Handwerker, D. A.; Molfese, P. J.; Ejima, Y. Sadato, N.; Wu, J.; Bandettini, P. A. Layer-Specific Activation in Human Primary Somatosensory Cortex during Tactile Temporal Prediction Error Processing. NeuroImage 2022, 248, 118867.*

The human brain is hypothesized to continuously generate predictions of incoming sensory input and to calculate corresponding prediction errors from the perceived inputs to update internal predictions. In human primary somatosensory cortex (area 3b), different cortical layers are involved in receiving the sensory input (L3) and computation of error signals (L2/3 and L5/6). It remains unknown how the layers in the human area 3b contribute to temporal prediction error processing. To investigate prediction error representation in the area 3b across layers, we acquired layer-specific fMRI data at 7T from human area 3b during a task of index finger poking with *no-delay, short-delay and long-delay* touching sequences, shown in Figure 2.

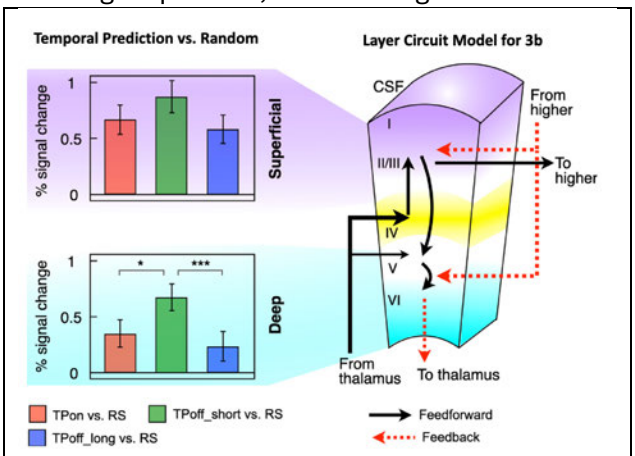


**Figure 3.** VASO signal changes in superficial and deep layers of human cortical area 3b and a layer-specific circuit model. The bar graphs shows the average activity changes in superficial layers and deep layers. Activity in the deep layers was enhanced by temporal prediction errors in the TPoff_short task, but these laminar effects were inhibited when the stimulation was delayed for a longer time (i.e., TPoff_long task).

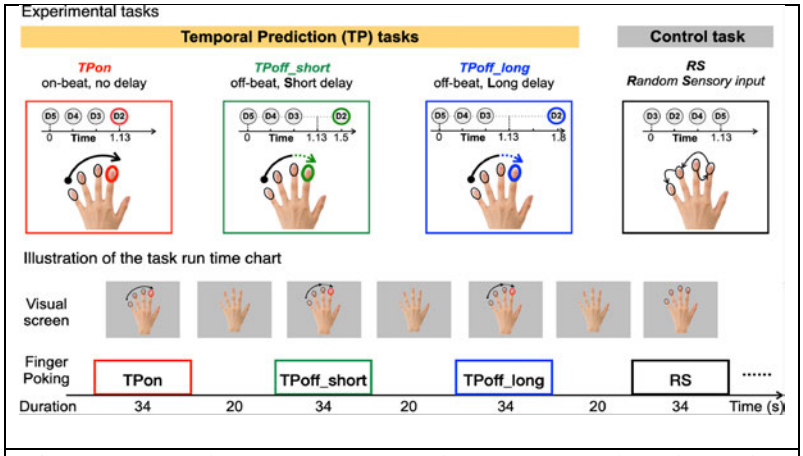


**Figure 2:** Experimental tasks and time chart. Tactile stimulation sequences of the three temporal prediction (TP) tasks and the random sensory (RS) input control task. In the three TP tasks, the fingers were stimulated in set order (pinky to index), with the index finger receiving stimulation with the same interval as the other fingers (on-beat). In the TPoff_short and TPoff_long tasks, index finger stimulation was delayed by one beat (approximately 0.37 s) or by two beats (approximately 0.74 s), respectively. In the RS task, fingers were stimulated in a random order.

Slice-selective simultaneous measures of blood volume changes and blood oxygenation changes using simultaneous VAscular Space Occupancy (VASO) and Blood Oxygen Level Dependent (BOLD) contrast acquisition were acquired at 7T using a 32-channel RF coil and an SC72 body gradient coil. The VASO-relevant acquisition was as follows: $TI1_{nulled}$ = 1100 ms, $TI2_{BOLD}$ = 2845 ms, and $TR_{pair}$= 3490 ms. The resolution was 0.71 mm across cortical depths with 1.8-mm thick slices perpendicular to the postcentral bank of the right central sulcus. 3D-EPI VASO contrast was corrected for BOLD contaminations by the division of blood nulled MR-signal and not-nulled MR-signal across consecutive TRs. The higher detection sensitivity of BOLD (with low layer specificity) was used to determine the single-voxel activity scores for region of interest analysis. The higher layer specificity of VASO (with lower sensitivity) was used to extract layer-profiles of voxel-averages for each layer without venous contamination.

We demonstrate that all three tasks increased activity in both superficial and deep layers of area 3b compared to the random sensory input. Figure 3 shows that the activity across the three contrasts revealed an inverted V-shaped activity primarily in the deep layers that was dependent on the length of the delay between middle and index finger poking, with enhanced activity, relative to the expected stimulus at the expected time (TPon), in the deep layers during the short delay period of 0.37 sec (TPoff_short) but reduced during the longer delay period of 0.74 sec (TPoff_long). The functional segregation in area 3b across layers may reflect excitatory and inhibitory interplay in the sensory cortex, with thalamus providing inhibitory input with longer delays.

### 1.3 Ultra-High Resolution Registration and Rapid T1 Mapping Using the T1234 Pulse Sequence

*Kan, C. K.; Stirnberg, R.; Montequin, M.; Gulban, O. F.; Morgan, A. T.; Bandettini, P.; Huber, L. R. T1234: A Distortion-Matched Structural Scan Solution to Misregistration of High Resolution fMRI Data. bioRxiv* ***2024****.*

A survey by the ISMRM brain function study group found that the most limiting factor of high-resolution fMRI is image registration despite the fact that researchers commonly invest significant time (≈10 min) in acquiring high-quality anatomical data with MP2RAGE2. In this study, we present a novel acquisition method: T1234, involving T1-weighted acquisition with 2 inversions of 3D-EPI and 4 directions through k-space which provides distortion-matched, high anatomic contrast, and artifact mitigated structural reference data in 3:40 min.

We tested T1234 in twelve MRI sessions (7 participants) across three 7T scanners in our center. Scan parameters were: 0.8mm, Skipped-CAIPI, matrix 232x232x186. We used a high segmentation factor to minimize distortions and T2*-blurring. A single volume of a bias-field corrected T1-weighted signal is reconstructed from pairs of TIs. Besides increased SNR through averaging, the following corrections are facilitated:

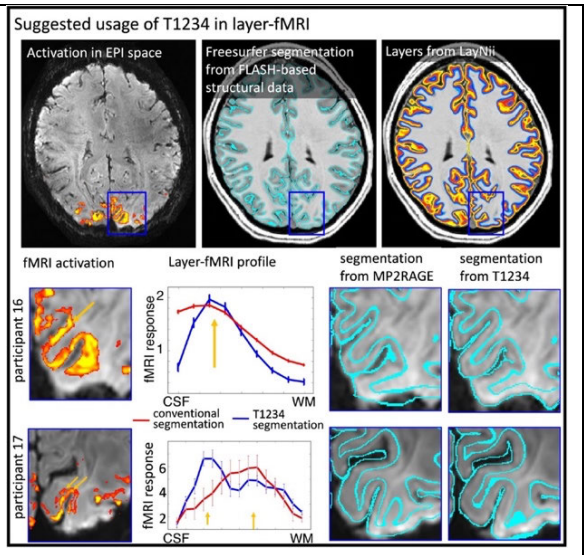


**Figure 4:** Imperfect image alignment layer profiles are compromised when using FLASH based structural images. Layer activation patterns that follow the cortical ribbon at unique cortical depths are shown in the bottom left. When these signals are pooled from misregistered data, the depth-dependent peaks are blurred. When segmentation borders have higher spatial precision from T1234 data, the peaks of depth-dependent activations become visible in layer profiles.

Of the four images produced, two images associated with opposite *read* directions mitigate low frequency EPI shadows known as "Fuzzy Ripples" that have been shown to arise from imperfection of k-space trajectories and off-resonance effects. Two images associated with opposite *phase* encoding directions show opposite distortions. The adjustable level of segmentation and phase bandwidth in T1234 can then be matched to the effective echo spacing of the functional data, thus matching all distortions on the acquisition level. Having these distortions in opposite directions allows the researcher to estimate the distortion field to retrospectively synthesize any desired level of geometric warping. In two participants, we also tested the acquisition of a single phase encoding direction, while keeping the effective echo spacing identical to a conventional fMRI protocol. Figure 4 summarizes these advantages.

The method also has potential to map unique functional contrast based on T1 or perhaps bulk tissue volume changes with activation. We modified the above acquisition to collect whole-brain T1 maps in 20-40 seconds using highly segmented 3D-EPI inversion recovery sequences to generate two T1-weighted scans for MP2RAGE-like image processing. This method enabled us to capture Freesurfer-estimated apparent gray matter (GM) thickness within timeframes compatible with fMRI task blocks. Three 12-min runs of checkerboard stimulation with four TIs and IR-TRs of 3.8 sec. Preliminary results show task-induced increases the volume of activated brain areas by 10-20%, while non-active regions remained stable. Our findings reveal that most GM expansion occurs at the GM/white matter (WM) boundary.

## 1.4 Layer Analysis Tools: Patch Analysis and Layer ReHo

*Burak Akin, Renzo Huber, Dan Handwerker, Peter Bandettini*

In recent years, members of SFIM and collaborators have developed a software suite, called LayNii[3] that addresses the challenges unique to layer fMRI. Visualization and projection of data into a dimension where it can be directly assessed is of increasing importance as fMRI reveals transient correlated activity along cortical layers. We describe two tools here. The first tool, shown in Figure 5, addresses the need to analyze the dynamics of layer activity over times scales achievable by acquisition limits. We call our approach **"patch analysis."** It focuses on both cortical

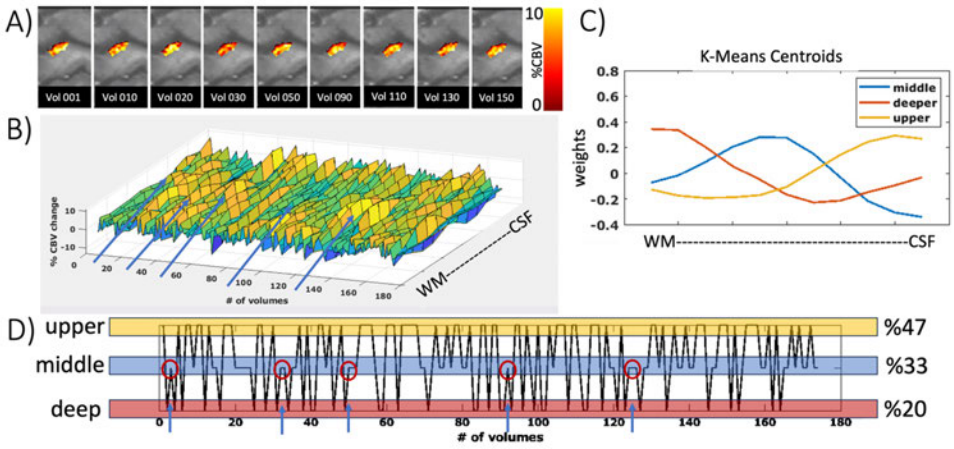


**Figure 5.** Sample patch analysis of an index finger area to a tactile stimulation. A) Instantaneous CBV patterns of right index finger area, B) Patch representation of the depth dependent activity over time C) three main Centroids of the K-Means clustering. D) Cluster indices of every instantaneous layer profile, yellow for upper, blue for middle, red for deeper. Also, blue arrows indicating the time of tactile stimuli introduced to the index finger, corresponding to middle layer activity.

depth and time information associated with a given cortical patch - allowing direct viewing of layer profile changes in time, different analysis approaches such as ranking feedback and feed forward activity and capturing time instances of a specific layer or layer activation sequence in time, corresponding to an event.

The second tool considers the laminar stratification of function and determines the functional borders within a cortical ribbon by calculating the similarity of the laminar time series between all pairs of voxels within a segment of cortical ribbon. It is a model free and rapidly implemented tool for exploring any layer data, shown in Figure 6.

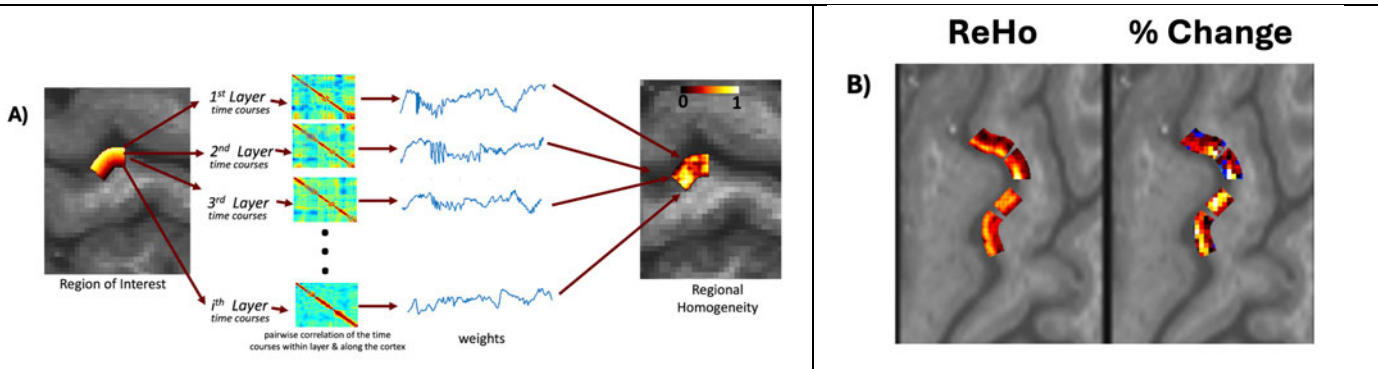


**Figure 6. A)** Layer dependent ReHo (Regional Homogeneity) calculation. Time courses are extracted from the same laminar bin and correlation coefficients across all pairs are calculated. A square matrix with a size of the number of voxels is averaged for each column, providing a weighted ReHo value of that voxel. **B)** Comparison of Layer ReHo maps with average CBV changes to tactile stimuli. On left, Regional Homogeneity of four different finger areas in which higher values show more homogeneous pattern. On right, average CBV change in finger areas are shown in percent signal change (+/- 10%).

# Theme 2: Fluctuations and Connectivity

## 2.1 Manifold Dimensionality Estimation for Resting State and Activation

*Gonzalez-Castillo, J.; Fernandez, I. S.; Lam, K. C.; Handwerker, D. A.; Pereira, F.; Bandettini, P. A. Manifold Learning for fMRI Time-Varying Functional Connectivity. Frontiers in Human Neuroscience 2023.*

Whole-brain fMRI connectivity (*FC*) evolves at temporal scales from seconds to years. This time varying functional connectivity (tvFC) has high dimensionality that defies efficient processing. Here we aim to find the most meaningful low dimensional representations to retain the most salient brain activity information for resting state and task data. In this study we explore low dimensional manifolds of tvFC data by estimating their intrinsic dimension (ID), which is defined as the minimum number of latent dimensions. We then characterize three state-of-the-art approaches: Laplacian Eigenmaps (LEs), T-distributed Stochastic Neighbor Embedding (T-SNE), and Uniform Manifold Approximation and Projection (UMAP). For each method, we evaluate its ability to generate neuro-biologically meaningful representations, as well as their robustness to hyper-parameter selection. Figure 7 summarizes our findings. Our results show that tvFC data has an ID between 4 and 6, and that rest states have a significantly higher ID. We also show how all three methods can capture subject identity and task: UMAP and T-SNE can capture these two levels of detail concurrently, but LE could only capture one at a time. While manifolds can generate summary views of task-labeled tvFC data, their application to unlabeled data such as resting-state remains a challenge.

Regarding dimensionality, our results show that tvFC data has an ID that ranges between 4 and 6, suggesting that the dimensionality of tvFC can be aggressively reduced and still preserve salient properties of the data (e.g., task and subject identity). They also show that the ID of tvFC from rest periods is significantly higher than that of the other

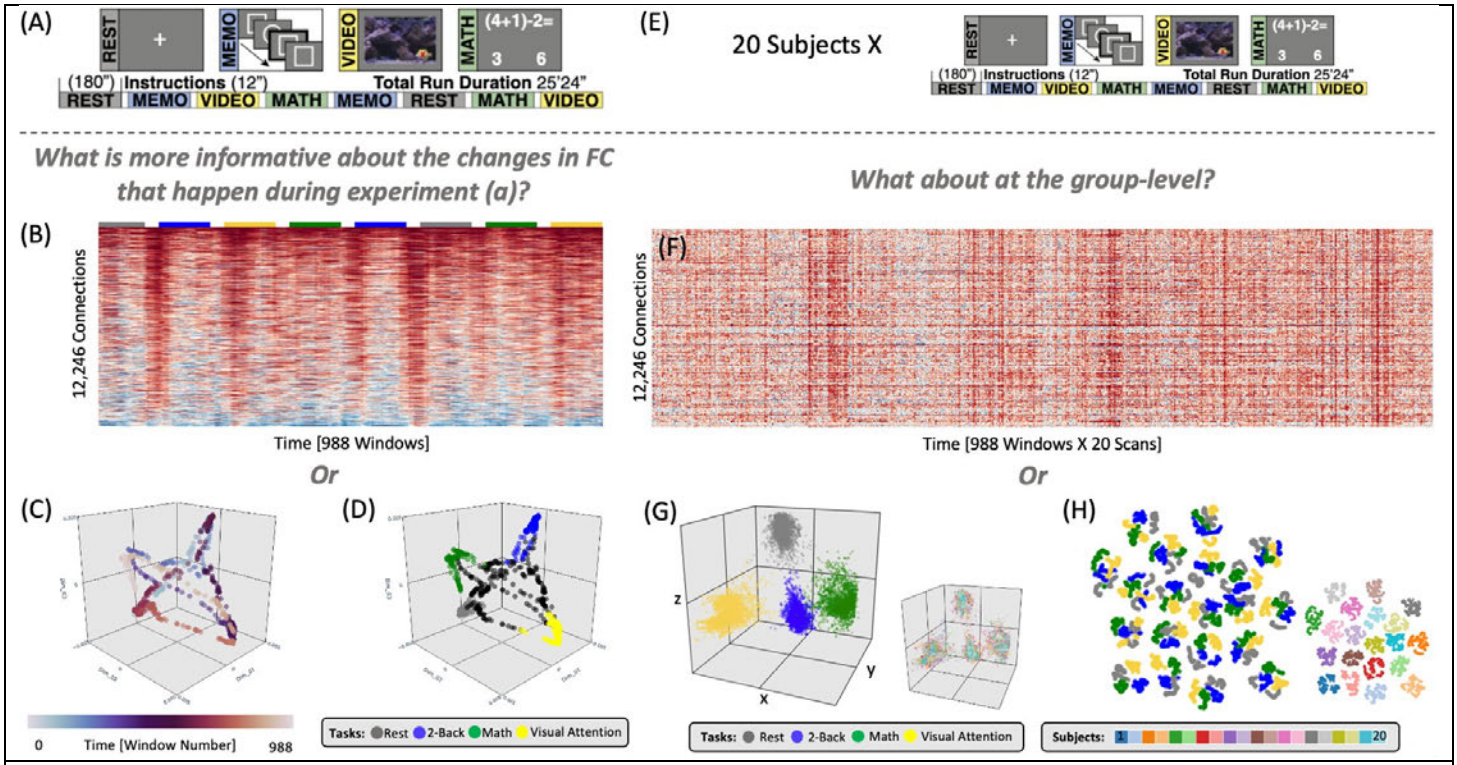


**Figure 7**. (A) Experimental Paradigm. (B) tvFC matrix for one scan. (C) Laplacian Embedding for the scan in (B). Each dot represents a column in the tvFC matrix. Dots are annotated by time from scan onset. (D) Same as (C) but annotated by task. Black dots indicate windows spanning across tasks and/or instruction periods. (E) Group schematic. (F) Concatenation of all 20 tvFC matrix into one. (G) Scan-level Laplacian Eigenmap + Procrustes group embedding. that captures task structure. (H) UMAP group embedding that captures both subject identity and task structure. (G) and (H) show embeddings annotated with task (big) and subject identity (small).

three tasks, suggesting that FC traverses a larger space of possible configurations during rest compared to when subjects are engaged in tasks with more precise cognitive demands.

Regarding benchmarking, we evaluated embedding quality based on task separability to mimic two common uses in neuroscience: exploration of group structure in the data (e.g., FC states, populations) and generation of input features for classification (e.g., biomarker development). In summary, tvFC data can be meaningfully summarized with two or three dimensions; however, obtaining *2D/3D* embeddings, especially for resting state data, requires careful hyper-parameter selection and larger datasets. For resting state data, where labels are missing, an empirical approach based on multi-task data might be an effective alternative for derivation of optimal hyper-parameters.

## 2.2 Edge Analysis: Duration and Variability

*Josh Faskowitz, Javier Gonzalez-Castillo, Peter Bandettini*

The time-varying nature of functional connectivity provides an avenue to understand brain dynamics. Previous research on time-varying connectivity, explored using sliding window analysis or power spectrum analysis has framed temporal fluctuations as relatively smooth - tracking how particular patterns unfold over the course of several seconds or how the brain might occupy different states over the course of seconds, minutes, or even longer.

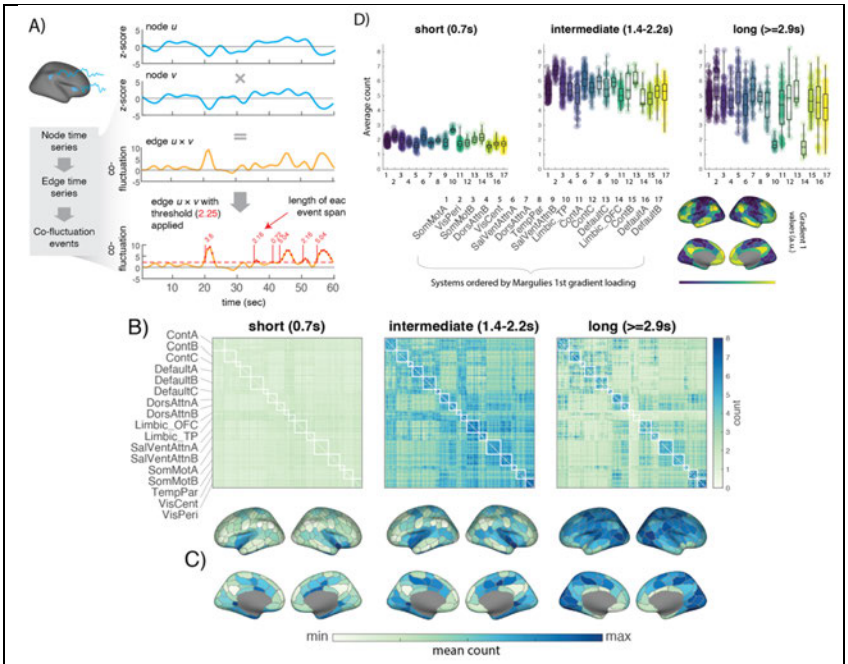


**Figure 8: A)** An illustration of edge time series construction and how high-amplitude edge events are defined; note the various supra-threshold event lengths. **B.)** Average count matrices (N=176) for each event category (short, intermediate, long); canonical systems are highlighted by the on-diagonal white squares**. C)** Average count data projected to the surface nodes by summing the matrices in panel B across rows, creating network degree maps: short activity concentrated in Limbic regions; long activity in Visual and Dorsal Attn. nodes. **D)** Average count data loading onto canonical networks; networks ordered on x-axis by rank on principle gradient; one-way ANOVA for difference in means significant for each category.

New methods have emerged that can resolve temporal fluctuations at the resolution of the collected data.[4] Using these methods that avoid temporal smoothing associated with sliding window analysis, variation of functional connectivity has been shown to be marked by transient (< 5 sec) moments of high amplitude activity[5]. These moments, by themselves, have been shown to fully capture most of the brain's dynamic correlation structure[6] and canonical functional networks[7,8]. Such brief, high amplitude events, constituting as little as 3% of the entire time series, are the primary source of functional connectivity across a time series[9].

When we identify a high amplitude event, are there any features that would delineate it from other events? Previous point-processes fMRI studies treat events equally. Here, we classify events based on the duration above a threshold, allowing us to classify events into temporal categories (short, intermediate and long duration). With this added information, we can probe for functional organization at each timescale. We can also ask how functional relationships with similar correlation magnitudes might exhibit different temporal event patterns. We seek to add beyond that of correlation, to probe the complexities of cortical interaction.

This study used a quality-controlled subset of subjects from the Human Connectome Project (HCP) fMRI data release[10]. Node time series were constructed by averaging functional data within 200 nodes of the Schaefer parcellation[11]. Edge time series were constructed by taking the element-wise product between two z-score node

time series (Fig. 8A). For each time series, supra-threshold moments were defined as edge time series magnitudes exceeding 2.25. This threshold was determined as the level yielding the highest correlation between event count and correlation, on average, across subjects. The number of time points spent supra-threshold contiguously was recorded as the duration. Next, event duration variability was calculated as the mean-absolute deviation of durations at each edge. This feature reflects the temporal consistency between regions (e.g., is connectivity unfolding with the same event lengths or a range of lengths over time?).

Brain organization formed by counting the short (0.72 sec), intermediate (1.4-2.2 sec), and long (>=2.9 sec) events was assessed as an adjacency matrix (Fig. 8B), a weighted degree map (Fig. 8C), and as loadings onto canonical functional system (Fig. 8D). Short spikes appear to preferentially include limbic nodes, including the orbitofrontal and temporal poles, as well as along the midline cingulate. Intermediate spikes are the most common, and load heavily onto limbic and ventral attention networks. The long spikes involve nodes of the visual cortex and generally involve areas on the primary sensory end of the macroscale gradient of functional organization[12] (Margulies, 2016). Long spikes appear mostly within-network and between the sensory network and salience networks. Further, we compare edge time series mean with event duration variability (Fig. 9A), to map a set of edges that have relatively low and high variability despite sharing a similar static functional connectivity (Fig 9B). We find that edges of the peripheral visual cortex are specifically more variable, based on a randomization test (spin-test).

By comparing event duration, we demonstrate that edges of similar average correlation can indeed have quite diverse patterns of short-term communication. Furthermore, we find that longer, and more variable events primarily involve somatosensory areas, and the primary visual system. These regions' role is the processing of external stimuli. That they exhibit highly variable communication patterns during rest (i.e., lacking such external stimulation) suggests they also play an active role in spontaneous brain process that have unknown cognitive/biological. using this approach, we may shed light on the information within the temporal properties of network engagement.

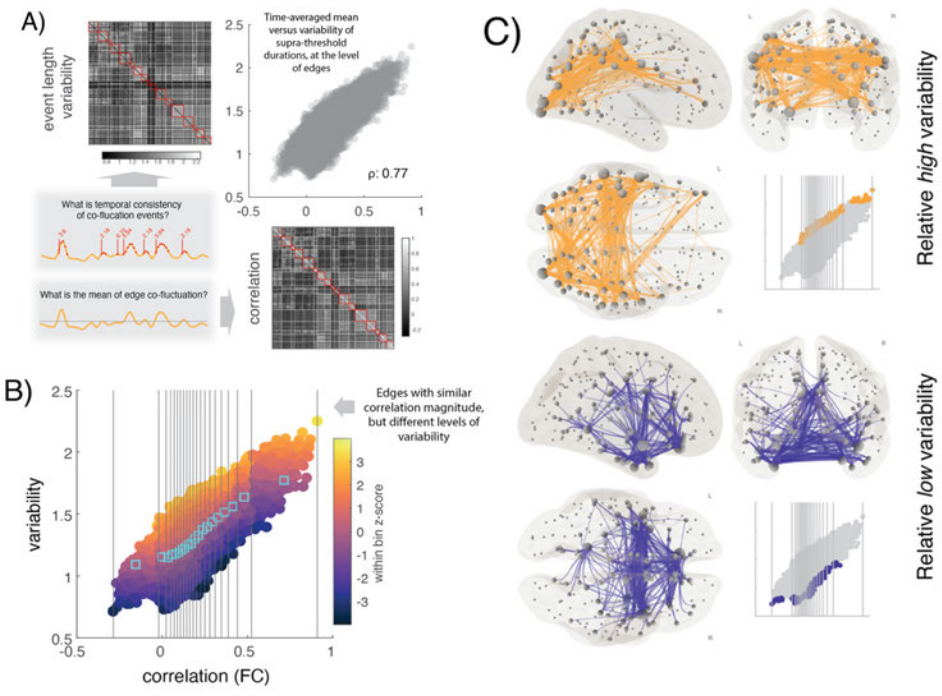


**Figure 9: A)** Edge time series can be summarized using the mean across time (x-axis; which is mathematically equivalent to the Pearson correlation), or the variability of the event duration times (y-axis); such features are positively correlated. **B)** The relationship between edge time series mean and temporal variability can be probed by binning the x-axis into centiles of 5% (20 bins total), and z-scoring the variability values within each bin to render a relative variability score indicted by the color of each scatter point; blue squares = bin mean **C)** The highest (top) and the lowest (bottom) 1% of the relative variability scores, visualized as edges on a smoothed glass brain; high edges connect visual nodes to Control and Dorsal Attention networks.

## 2.3 Intersubject Correlation Analysis (ISC) Identifies Neural Correlates of Reading Ability

*Jangraw, D. C.; Finn, E. S.; Bandettini, P. A.; Landi, N.; Sun, H.; Hoeft, F.; Chen, G.; Pugh, K. R.; Molfese, P. J. Inter-Subject Correlation during Long Narratives Reveals Widespread Neural Correlates of Reading Ability. NeuroImage 2023, 282, 120390.*

Inter-subject correlation (ISC) analysis has emerged as a powerful approach to analyzing naturalistic data, as it provides several advantages over traditional model-based linear regression techniques. ISC analysis measures task-evoked brain activity over the course of a naturalistic stimuli time course by taking one subject's signal as a model for a second subject's signal at the same spatial location[13] Rather than attempting to fully model every dimension of a naturalistic stimulus or task, ISC simply asks the question of how similar one subject's response is to another when presented with an identically timed stimulus or task, thus leveraging all of the induced fMRI signal for subject comparison rather than precisely delineating the neuronal correlates.

Recent work using fMRI ISC analysis has provided insight into the brain's response to video and audio narratives, showing frontal activation not typically activated by single words. This approach is well suited to the study of reading, where narrative is central to natural experience. Past reading paradigms have presented single words or phrases, so the influence of narrative on semantic processing in the brain – and how that influence might change with reading ability – remains largely unexplored.

In this study, we presented stories to adolescents and young adults with a wide range of reading abilities. The stories were presented in alternating visual and auditory blocks. We used ISC analysis to identify regions in which better and worse readers had varying levels of consistency with other readers. This analysis identified a widespread set of brain regions in which activity time courses were more similar among better readers than among worse readers, as

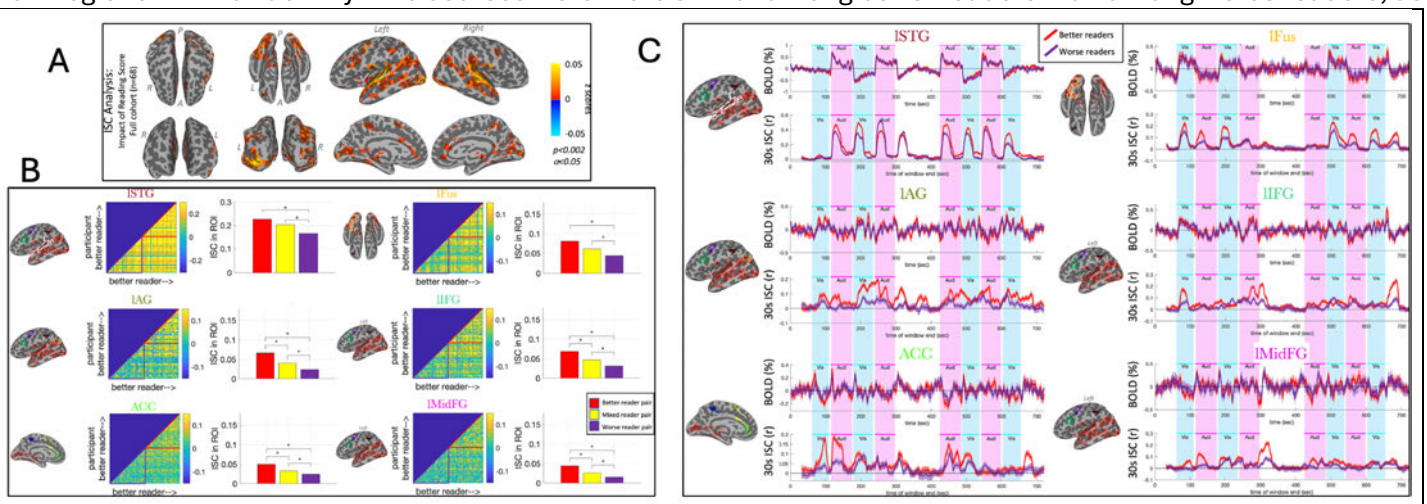


**Figure 10: A.** Clusters showing a significant impact of reading score on ISC in the full cohort ($n$ = 68). Block GLM analyses (not shown) showed no significant group differences**. B.** Pairwise ISC in select clusters. A subset of the clusters showing a significant impact of reading score on ISC in our full cohort ($n$ = 68) are shown here. Each cluster has a pair of plots with a title whose color matches the corresponding cluster seen on the brain to its left. Subjects are sorted according to their composite reading score, such that better readers are closer to the top and farther to the right. Colored triangles mark the median-split groupings into better reader pairs (red) and worse reader pairs (purple). Right: mean pairwise ISC among two better readers ("better"), one better reader and one worse reader ("mixed"), and two worse readers ("worse"). Stars indicate group differences were significant in permutation tests at $p$<0.05 (uncorrected). **C.** Time-courses of activity and ISC in select clusters with significant impacts of reading score on ISC in the full cohort ($n$ = 68). Each cluster has a pair of plots with a title whose color matches the corresponding cluster seen on the brain to its left. Outlines indicate the largest cluster's overlap with a language region derived from an atlas. Below each title, we see at the top the mean BOLD time-course across better readers (red) and worse readers (purple) in the cluster. Below this is the mean pairwise ISC in a 30-second window ending at each time point (i.e., the value at each time is the ISC in the previous 30 s). Patches represent standard error of the mean. The magenta and cyan bars behind each plot show the times when auditory and visual stimuli were being presented (these times are offset 6 s to account for typical hemodynamic delays).

summarized in Figure 10. These differences were not detected with standard block activation and linear regression analyses and subsequent comparisons. Worse readers had "idiosyncratic" responses, not resembling each other, hypothetically manifesting multiple compensatory mechanisms. These differences were not explained by differences in IQ or motion and expand the current view of where and how reading ability is reflected in the brain. Furthermore, these results establish inter-subject correlation as a sensitive tool that has opened up further avenues of research for reading disorders.

# Theme 3: Multi-modal Integration

## 3.1 Task Engagement during Drowsiness

*Kumar, S. S.; Arzi, A.; Bareham, C.; Gonzalez-Castillo, J.; Fernandez, I.; Tagliazucchi, E.; Mediano, P. A.; Bandettini, P. A.; Bekinschtein, T. A. Brain Network Dynamics in Transitions of Consciousness Reorganize According to Task Engagement. bioRxiv* ***2023****, 2023–06.*

Substantial changes in behavior, physiology, and brain function occur when alertness decreases. These changes in brain function involve increased synchronization between cortical areas as well as alterations in sensory processing pathways and networks connecting the thalamus and cortex. Cognitive tasks engage overlapping functional networks with sensory pathways facilitating information processing, and thalamocortical and corticocortical networks supporting task performance. Frontoparietal circuits play a crucial role in cognitive tasks and states of decreased consciousness. To develop an integrated framework of consciousness and cognition, it is important to understand how fluctuations in alertness and cognitive processing interact in these shared circuits. Our hypothesis is that during periods of low alertness, individuals who actively maintain task engagement would recruit additional frontoparietal and sensory processing networks, while thalamocortical dynamics that typically change during sleep onset would remain unaffected. Figure 11 summarizes our findings. We characterized how auditory, thalamocortical, and frontoparietal networks change during decreasing alertness across two different levels of task engagement. We identified changes that were 1) common to both passive listening and active task engagement, 2) specific to active task engagement, and 3) specific to passive listening. Healthy adult participants listened to binaural auditory tones during simultaneously acquired electroencephalography (EEG) and functional magnetic resonance imaging (fMRI) (EEG-fMRI). In the *Active* task, participants (N=20) indicated whether each tone was heard to the left or right of their midline using a button box, and in a *Passive* task, participants (N=20) passively listened to the tones with no motor response required. We extracted the fMRI timeseries for 188 cortical brain regions of interest (ROIs) grouped into six networks (i.e., Visual, Auditory, Somatomotor, Dorsal Attention, Ventral Attention, Control, and Default Mode Network (DMN)), and two ROIs for the left and right

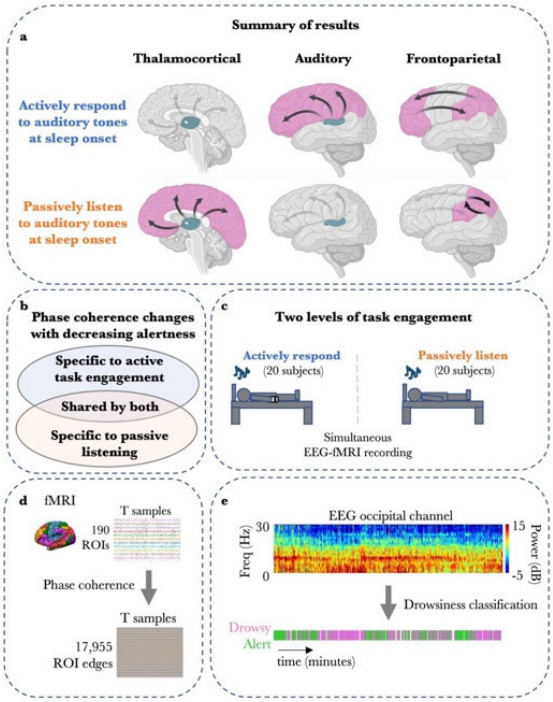


**Figure 11. Summary, experimental design, and analysis: a**. At sleep onset, the *Active* task is associated with unchanged thalamocortical dynamics, as well as increased auditory-cortical and frontoparietal synchronization. The *Passive* task is associated with increased thalamocortical and parietal synchronization, and auditory-cortical dynamics are relatively unchanged. **b**. We explored changes in fMRI phase coherence that are specific to each level of task engagement and changes that are shared by both levels of task engagement. **c**. Two separate groups of participants underwent EEG-fMRI recording while listening to auditory tones. One group actively responded to the tones while the other group passively listened. **d**. The fMRI timeseries for 188 cortical and 2 thalamic ROIs were extracted, and the instantaneous phase coherence was calculated between each pair of ROIs at each timepoint. **e**. EEG data epochs were classified as alert or drowsy.

thalamus. At each timepoint, instantaneous phase coherence was calculated between each pair of ROI timeseries, resulting in one edge time course for each ROI pair. The concurrent EEG data were classified as alert or drowsy (i.e., high or low levels of alertness) on four-second epochs.

Our findings demonstrated that as alertness decreased, passively listening to auditory tones led to increased synchronization in the parietal lobe, whereas actively performing an auditory task resulted in increased long-range frontoparietal synchronization. During decreasing alertness, passive listening (but not active task engagement) was associated with widespread increased synchronization between the thalamus and cortex. In contrast, active task engagement (but not passive listening) led to increased synchronization between the auditory cortex and the rest of the brain. These results reveal the functional mechanisms of the brain's flexible reorganization during transitions of consciousness when individuals are actively engaged in cognitive processes.

### 3.2 Real-Time Pupil Size Measurement

*Kronemer, S. I.; Gobo, V. E.; Walsh, C. R.; Teves, J. B.; Burk, D. C.; Shahsavarani, S.; Gonzalez-Castillo, J.; Bandettini, P. A. Cross-Species Real-Time Detection of Trends in Pupil Size Fluctuation. Behavior Research Methods* ***2025****, 57 (1), 1–14.*

Pupillometry – the measure of pupil size – has grown in popularity with evidence that pupil size is an easily measured marker of neurophysiological activity. Shown in Figure 12a, neuromodulatory networks, including the locus coeruleus-noradrenergic and basal forebrain-cholinergic systems, are linked to changes in pupil size. These brain networks are also involved in regulation of cortical and subcortical regions. Therefore, pupillary dynamics can reflect both large-scale brain activity and behavioral, cognitive, emotive, and perceptual states that emerge by central neural mechanisms. Pupil size predicts states of locomotion, arousal, and conscious awareness.

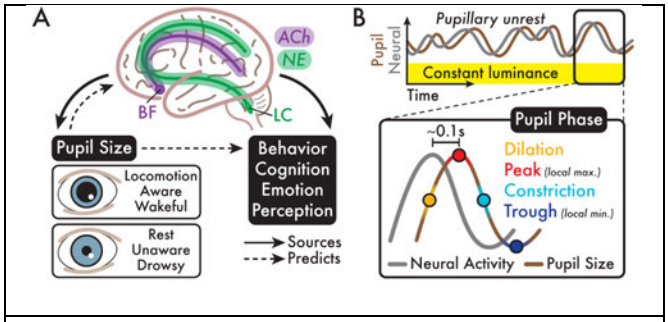


**Figure 12. Neural sources and phases of pupil size fluctuations**. **(A)** Major neuromodulatory networks, including the basal forebrain (BF) cholinergic system (ACh) and the locus coeruleus (LC) noradrenergic system (NE), broadly modulate subcortical and cortical activity. Spontaneous and evoked ACh and NE neural activity are linked with pupil size, enabling prediction of both brain activity and behavioral, cognitive, emotive, and perceptual states. In humans, dilated pupils indicate locomotion, awareness, and wakefulness, while constricted pupils indicate rest and drowsiness. **(B)** Pupillary unrest is the spontaneous fluctuation of pupil size independent of environmental luminance where pupil size or pupil phase are a delayed (0.1 seconds) indicator of neural activity.

We introduce *rtPupilPhase* – an open source software that automatically detects trends in pupil size in real time, enabling novel implementations of real time pupillometry towards achieving numerous research and translational goals. The performance of rtPupilPhase has been validated on human, rodent, and monkey pupil data and propose future applications of real time pupillometry.

There are many potential applications of rtPupilPhase. We are currently using eye metrics to study conscious awareness and brain activity in cerebral blindness. A promising future use is the development of closed-loop paradigms (e.g., the real time detection of pupil phases triggers task events). This approach allows for targeted testing and possible causal interpretations for the interaction among pupil size and phase, neurophysiology, and behavior. For example, a study found that increasing pupil size at the time of a stimulus corresponded with improved perceptual performance[14].

Future experiments could extend on this finding by testing if pupil phase predicts perceptual-sensitivity by presenting near-threshold stimuli timed with target pupil phase events. Concurrent neuroimaging recording could help deduce the mechanisms underlying changes in behavioral performance (e.g., perception rate and reaction time) linked with pupil phase. An alternative application of rtPupilPhase is as a tool for pupil biofeedback. A recent study found participants can self-regulate absolute pupil size[15]. Using rtPupilPhase, participants could receive real time input of their pupil phase to regulate their pupillary fluctuations. Modifying pupil phase states may alter arousal, salience, and attention, with effects on behavior, cognition, emotion, and perception.

### 3.3 Wide Field Optical Imaging of Concordant Neuronal and Hemodynamic Activity

*Shahsavarani, S.; Thibodeaux, D. N.; Xu, W.; Kim, S. H.; Lodgher, F.; Nwokeabia, C.; Cambareri, M.; Yagielski, A. J.; Zhao, H. T.; Handwerker, D. A.; Gonzalez-Castillo, J.; Bandettini, P. A.; Hillman, E. M. C. Cortex-Wide Neural Dynamics Predict Behavioral States and Provide a Neural Basis for Resting-State Dynamic Functional Connectivity. Cell Reports 2023, 42 (6).*

A central question in fMRI that remains to be fully answered is the precise temporal and spatial relationship between hemodynamic signal changes and neuronal activity. In this collaborative study, progress was made towards addressing this question. A wide-field optical mapping (WFOM) approach was used to simultaneously record pan-cortical neuronal and hemodynamic activity in awake, spontaneously behaving mice. Leveraging fluorescent calcium indicators expressed in excitatory neurons, WFOM has previously been used to demonstrate that resting-state hemodynamics in the brain of awake mice can be largely predicted by baseline fluctuations in the excitatory neuronal activity[16]. Here, we leverage improved, red-shifted calcium indicators in cortical neurons to visualize these neuronal patterns with a higher spatiotemporal resolution. We combine this imaging of neuronal activity with simultaneous mapping of cortical hemodynamics and detailed recordings of spontaneous behavior and pupil dynamics in awake mice to analyze the relationship between real-time brain activity, brain state, and behavior, as shown in Figure 13.

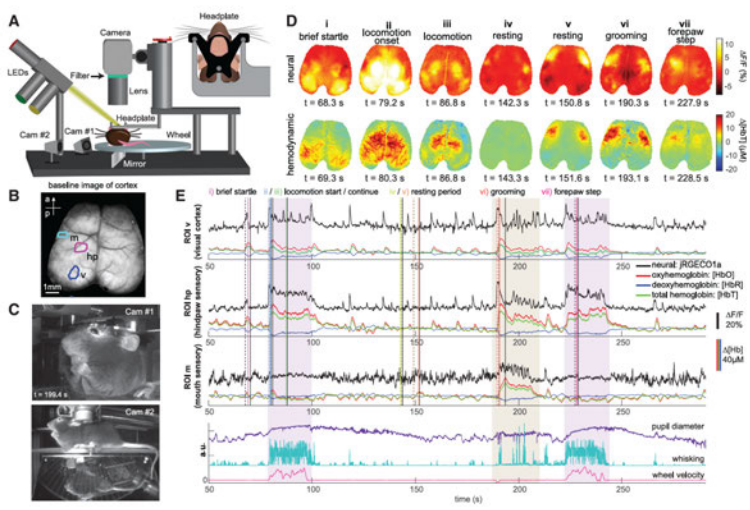


**Figure 13.** Imaging setup and raw data images and signals (A) Schematic of wide-field optical mapping (WFOM) system. The mouse is positioned on a freely moving horizontal wheel with dual-camera behavioral monitoring, and a head-fixation plate surrounding the thinned-skull cranial window. (B) WFOM camera field of view showing raw image. (C) Behavior camera 1 captures the face, mouth, pupil, and forepaws. Camera 2 captures the side and underside of the mouse via an angled mirror. (D) Top, neural (D% fluorescence change after hemodynamic correction) and bottom, total hemoglobin (DHbT) images corresponding to specific events listed. (E) Neural and hemodynamic time courses extracted from mouth(m), forepaw(fp), and visual(v) ROIs indicated in (B). The coupling between neural activity and hemodynamics, increasing HbT and HbO and decreasing HbR, can be clearly observed for small and large events.

Correlations between neural activity showed stable patterns when averaged over 10 minute epochs; however, also displayed shifts in the patterns across all time scales, as shown with dynamic resting state fMRI. These dynamic patterns also showed consistent changes associated with spontaneous locomotion as well as changes in arousal during rest. Reduced arousal level was accompanied by an increase in the amplitude of neural fluctuations, predominantly in the anterior lateral frontal cortex, reducing the correlation between anterior and posterior brain regions. Repeating the same analysis on simultaneously recorded hemodynamic data revealed similar patterns associated with behavioral state transitions. If stronger synchronization, or functional connectivity between cortical brain regions can be considered as a measure of the information integration, then our findings may indicate reduced multisensory integration during periods of quiescence.

Comparison of neural and hemodynamic signals confirmed that hemodynamics provide a temporally low-pass filtered representation of neuronal activity, even when neuronal signals were high-pass filtered to retain frequencies exceeding those represented by hemodynamics. These findings support the broadband nature of the neuronal activity underlying dynamic correlations and empirically demonstrate that lower-frequency hemodynamics are able to capture similar correlation features and transitions.

Some components of observed neuronal activity clearly represent sensory and motor function. However, particularly during quiet rest, strongly fluctuating patterns of activity across diverse brain regions contribute to interregional correlations. Dynamic changes in these correlations coincide with changes in arousal state as measured by pupillometry. Simultaneously acquired hemodynamics depict similar brain-state-dependent correlation shifts. These results support a neural basis for dynamic resting-state fMRI, while highlighting the importance of brain-wide neuronal fluctuations in the study of brain state.

### 3.4 Network Configurations Shaped by Predominant In-Scanner Thoughts

*Gonzalez-Castillo, J.; Spurney, M. A.; Lam, K. C.; Gephart, I. S.; Pereira, F.; Handwerker, D. A.; Kam, J. W.; Bandettini, P. A. In-Scanner Thoughts Shape Resting-State Functional Connectivity: How Participants Rest Matters. bioRxiv 2024, 2024–06.*

Rarely considered in resting state scans are systematic differences subjects' thoughts and feelings during the scan. To evaluate their possible influence, we used 471 publicly available rs-fMRI scans (Leipzig MPI-Mind, Body, Brain dataset) annotated with self-reports about the content and form of in-scanner thoughts, and perceived levels of wakefulness. Wide-spread differences in FC are observed between different in-scanner experiences.

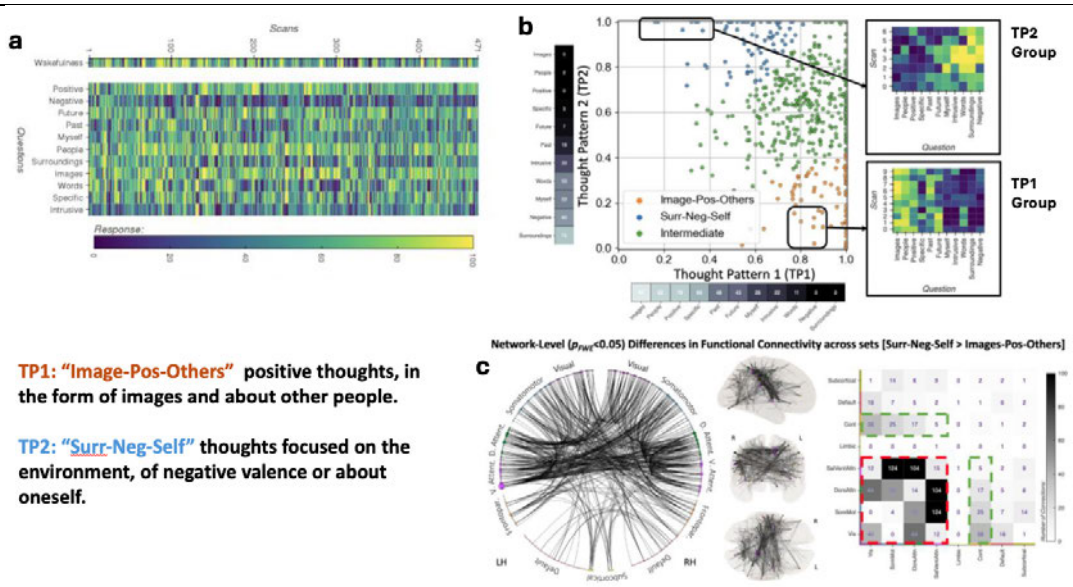


**Figure 14. a.** Responses to the experiential questionnaire (rows) for all 471 scans (columns). Top row corresponds to the "*wakefulness*" item. The matrix shows responses to the remaining 11 questions about the form and content of in-scanner thoughts. **b.** 2D representation of the self-reported data (except wakefulness). Here, each scan is represented by a colored dot. Axes represent two overall thought patterns extracted by the algorithm: X-axis (Thought Pattern 1 or TP1) represents positive thoughts in the form of images about other people, and Y-axis (Thought Pattern 2 or TP2) represents negative thoughts about the self and the surroundings. Dots representing scans are colored by set membership. To the right of the scatter plot, we depict answers for two groups of representative scans. On the top, we present answers for 7 scans with high loadings for TP2 and low loadings for TP1**. c.** Circos plot with connections rendered as significant for the TP2 > TP1 contrast. In this plot, ROIs are depicted as colored dots (color indicating network membership) on a circumference, and significant connections are depicted as black lines. ROIs are grouped by network and hemisphere. The size of the dot is proportional to the degree of the ROI. The same information is shown on a glass brain. ROI size denotes degree and color denotes network membership. To the far lower right: Counts of between- and within-network connections significant for the contrast TP2 > TP1.

Additionally, we show that FC can successfully predict specific aspects of in-scanner experience in a manner similar to how it predicts demographics, cognitive abilities, clinical outcomes and labels. Together, these results highlight the key role of in-scanner experience in shaping rs-fMRI estimates of FC. Figure 14a shows the responses to items about form and content of thoughts. We submitted these responses to the Interpretability Constrained Questionnaire Factorization (ICQF) algorithm, which generated a lower dimensional representation of the data in which each scan represented as a point in 2D space shown in Figure 14b. We subdivided our sample into groups

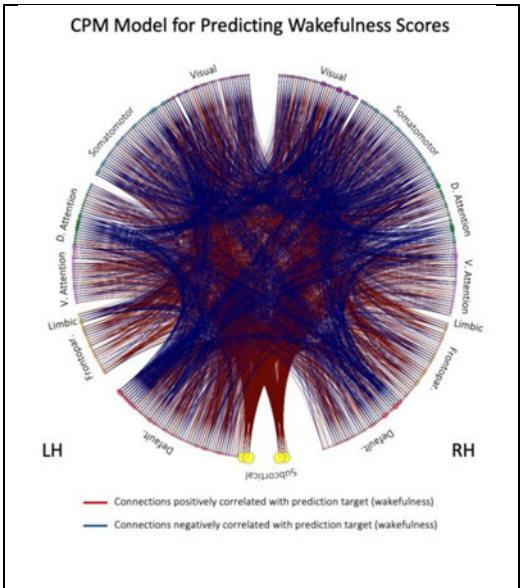


**Figure 15.** CPM model for Wakefulness, Circos plot depicting connections found to correlate positively (dark red) and negatively (dark blue) with the target.

with different in-scanner experience. TP1 is characterized by reporting thoughts in the form of images, of positive valence and about other people. TP2 is characterized by thoughts focused primarily on the environment and of negative valence. We estimated FC using the 400 ROI Schaefer Atlas augmented with 8 subcortical ROIs. As shown in Figure 14 c, significant differences in FC across groups were found. In all, 590 connections (0.82% of all possible connections) involving 221 nodes (58%) were stronger for the TP2 group than for the TP1 group.

To predict Wakefulness, the Connectome-based Predictive Modeling (CPM) framework[17] relied on a model that includes 3839 connections (5.3% of all possible connections) distributed across all seven networks 2026 (2.8%) of these connections exhibit positive correlation with the prediction target, and the remaining 1813 (2.5%) show negative correlation. A large fraction of the positively correlated connections represent links between subcortical and cortical regions, as shown in Figure 15. Conversely, connections that are negatively correlated with Wakefulness are cortex-to-cortex connections involving primarily the Default, Ventral and Dorsal Attention, and primary unimodal networks.

Figure 16 shows the CPM models for predicting factor scores on the two Thought Patterns previously described. The CPM model for TP1 is sparser (1036 connections | 1.4%) than the one for TP2 (1778 connections | 2.5%). For TP1, positively correlated connections involve nodes of the Frontoparietal Control and Default networks, with highest degree nodes sitting in bilateral dorsolateral prefrontal cortex (black arrows in Fig 16 b). Connections that correlate negatively with TP1 concentrate in central and posterior areas of the brain associated with Visual and Dorsal Attention networks. Highest degree nodes for this portion (negative correlations) of the model include the left medial intraparietal sulcus, part of the Dorsal Attention network, and left para-hippocampal area, part of the Visual network (black arrows in Fig 16 c). In summary, systematic differences in spontaneous thought pattern suffice to render significant differences in functional connectivity between groups of healthy subjects. Aspects of spontaneous thought patterns can be predicted from FC with accuracy levels like those previously reported for the prediction of cognitive, personality and clinical traits. Together, these results highlight a key, often overlooked, role of in-scanner experience in shaping rs-fMRI estimates of FC.

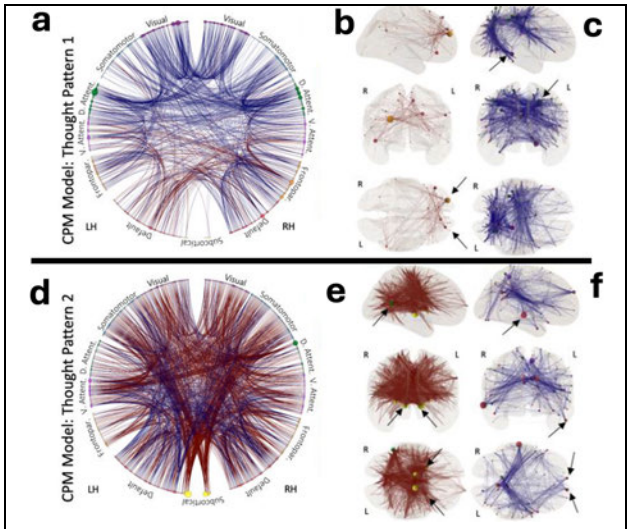


**Figure 16.** Prediction Model for TP 1 and 2. **a.** Circos plot of the CPM model for the prediction TP1 axis loadings. Dark red lines and dark blue lines denote, respectively, connections that correlate positively or negatively with the prediction target. **b.** Connections positively correlated with TP1. **c.** Connections negatively correlated with TP1. **d.** Connections positively correlated with TP2. **e.** Connections negatively correlated with TP1.

## 3.5 Cerebral Correlates of Low Frequency Photoplesmography (PPG) and Blood Pressure

*Joshua Dean, Burak Akin, Sharif Kronemer, A. Tyler Morgan, Dan Handwerker, Peter Bandettini*

The Photoplesmography (PPG) signal - a measure of light absorption from blood and collected from the fingertip - contains temporal features that resemble fMRI signal[18–20]. The PPG waveform has a non-pulsatile component in the range of < 0.1 Hz, which is associated with sympathetic activity and Mayer waves[20,21]. These slow wave components are referred to as low frequency oscillations (LFO) or systemic oscillations. Dynamic mean arterial blood pressure (MAP), a measure derived from tissue displacement with the heartbeat from a finger cuff, also likely has features

that are distinct from yet linked with PPG, and likely has a distinct temporal/spatial propagation pattern in the brain. In this study, we compare these two externally measured signal sources as regressors for fMRI time series - calculating maps of delay and correlation at the optimal delay.

Eleven healthy adult participants underwent a resting-state scan (14.8 ± 2.0 min) using a 7T multiband fMRI acquisition (TR=0.75s, TE=25ms, voxel-size=2mm isotropic, FOV=68 slices). fMRI data were motion-corrected, bandpass filtered (0.01-0.1 Hz), and normalized to Montreal Neurological Institute (MNI) space.

PPG traces were recorded using a pulse oximeter, BIOPAC MP160. A 4th order Chebyshev filter (fc = 0.1 Hz) was applied to each subject's PPG trace to compute the LFO regressors. Blood pressure signal over time was collected concurrently using CareTaker (BIOPAC). We determined the delay and optimal correlation on a voxel-wise basis of LFO or MAP with the fMRI signal by shifting the reference signal in 0.15s increments from f -10s to +30s.

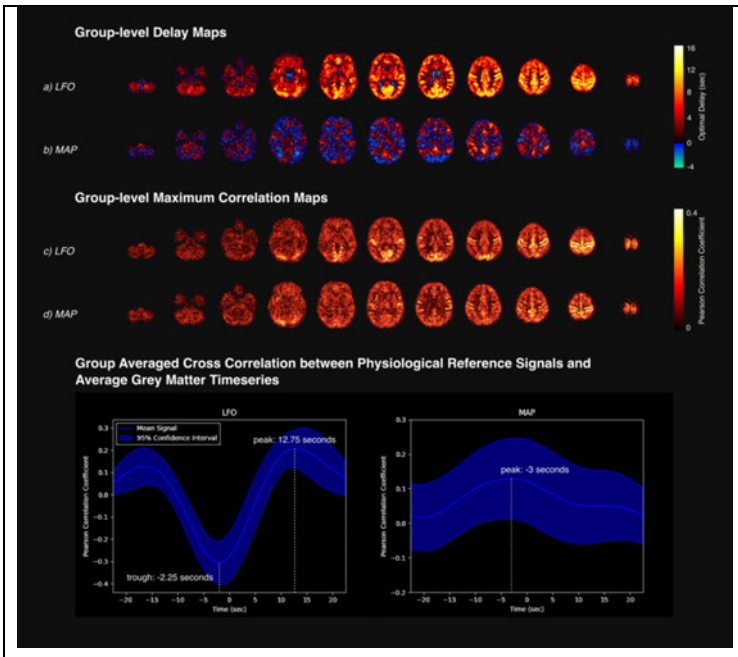


**Figure 17:** Group-averaged delay maps and maximum correlation maps using (a,c) LFO or (b,d) MAP as regressors. The correlation across a shifting lagged window of -30s to +30s between the LFO reference signal (bottom left) and MAP reference signal (bottom right) and the average gray matter time series is shown.

LFO and MAP are marginally anti-correlated (r = -0.1552 ± 0.1809), however they may also simply be time-shifted relative to each other. The delay maps produced using the MAP regressor are both weaker and show shorter delays than the delay maps produced using the LFO regressor as shown in Figure 17a-b. Both delay maps appear to follow perfusion density distributions, but MAP appears to highlight rapidly changing pulsatile regions. The LFO shows a more even distribution of slower changes, perhaps representing perfusion changes with changes in sympathetic tone. The correlation maps using the LFO regressor depict higher correlations in the visual cortex than MAP as shown in Figure 17c-d, which may suggest that visual input modulates LFO through sympathetic activity and subcortical control mechanisms.

The difference in the spatiotemporal signatures of LFO and MAP suggests that these coupled physiological fluctuations each provide their own unique information that may be intrinsically related to vascular density and patency, flow velocity, sympathetic tone, cerebral autoregulation, and other homeostatic mechanisms. Future research will aim to modulate these hypothesized relationships to perhaps determine causality, lending insight into BOLD fluctuations, opening up clinical applications, and perhaps improving the quality of BOLD connectivity measures by removing nuisance signals more effectively.

# Theme 4: Pulse Sequence Related Development

## 4.1 Towards Mapping of Cerebral Spinal Fluid Volume Changes

*Stephanie Swegle, Renzo Huber, Rudiger Stirnberg, Peter Molfese, Linqing Li, Catherine Walsh, A. Tyler Morgan, Peter Bandettini*

The manner in which Cerebral Spinal Fluid (CSF) acts as a clearance system in the human brain is currently unknown. Research has focused on determining changes of CSF flow and convection through the brain (i.e.

glymphatic system) during sleep, wakefulness, and brain activation[22,23]. Since CSF *flow* imaging is constrained by low velocities and directional dependencies, CSF *volume* imaging may be more easily detected and assessed. Here, we show our work aimed to develop, implement, and validate a new imaging approach to quantify changes of CSF volume across the human brain. We use a VASO-like inversion recovery (IR) sequence to capture CSF volume changes. Specifically, we have developed an inversion recovery 7T 3D-EPI protocol that uses the unique T1 and T2* relaxation "fingerprint" of CSF to capture voxel-wise CSF volume fractions independent of dynamic changes in cerebral blood volume (CBV) and blood oxygenation dependent (BOLD) signal.

We use a multi-echo multi-TI approach to quantify BOLD independent of $M_Z$ modulation of CSF to separate CBV changes from CSF volume changes. We collected images with three echoes and three inversion times at 7T as shown in Figure 18a (N=8 sessions at 7T (Siemens, Germany) with 8Tx/32Rx head coil (Nova, USA)). The TE, TI, T1 and T2* values that we used are shown in Figure 17b. The sequence was implemented in a 3D-EPI with Skipped-CAIPI framework). In-scanner eye tracking (EyeLink-1000Plus, SR-Research) and physiological monitoring (BioPack) were used. Images were processed using AFNI_24.2.01, LayNii_v2.7.0, SPM12, and FSL 1.12.4. We used an additive multi-compartment model to estimate functional contributions of CSF volume, CBV, and BOLD.

Figure 18 shows a diagram of the nested TE/TI cycling sequence as well as the simulated intensities of CSF and blood as a function of TI and TE. Depending on T1-weighting of CSF/CBV and T2*-weighting of BOLD, the fMRI contrast is modulated in polarity and strength. High resolution data, not shown, shows clear delineation of the expected spatial distribution of CSF and blood within and outside of the cortical ribbon. With brain activation, CSF-weighted signal changes are largest just outside the cortex, while CBV and BOLD show signal changes within GM. GE-BOLD exhibits a signal increase towards the cortical surface, as expected from draining vein effects.

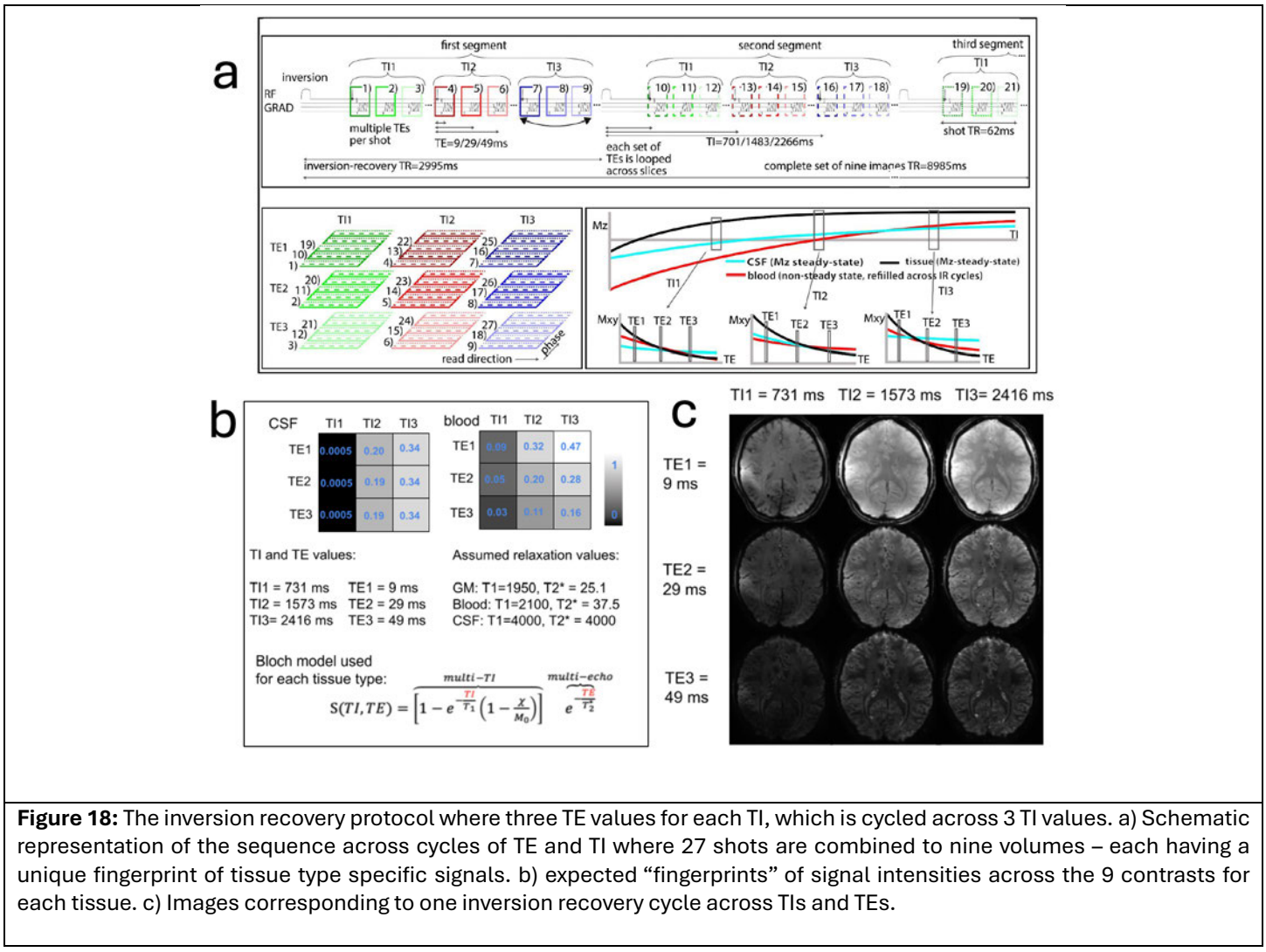


**Figure 18:** The inversion recovery protocol where three TE values for each TI, which is cycled across 3 TI values. a) Schematic representation of the sequence across cycles of TE and TI where 27 shots are combined to nine volumes – each having a unique fingerprint of tissue type specific signals. b) expected "fingerprints" of signal intensities across the 9 contrasts for each tissue. c) Images corresponding to one inversion recovery cycle across TIs and TEs.

We also monitored drowsiness during the scan using an eye tracker. Our preliminary results are shown in Figure 19. At events in which the eyes were closed (i.e. increased drowsiness) there was an almost immediate decrease in BOLD signal and an increase in the CSF signal. This signal returned to its previous state up opening of the eyes. This suggests that our sequence is uniquely sensitive to dynamic changes CSF distribution as well as BOLD contrast during transient fluctuations in vigilance, opening up a new window to study mechanisms of blood and CSF redistribution in the brain with varying levels of vigilance. Such a sensitive marker may have clinical impact as CSF flow pathology has been associated with neurologic and psychiatric pathologies. We intend to explore CSF dynamics with task modulation and with tracking across sleep stages. We also aim to determine how these dynamics change with behavioral modulations and patient populations.

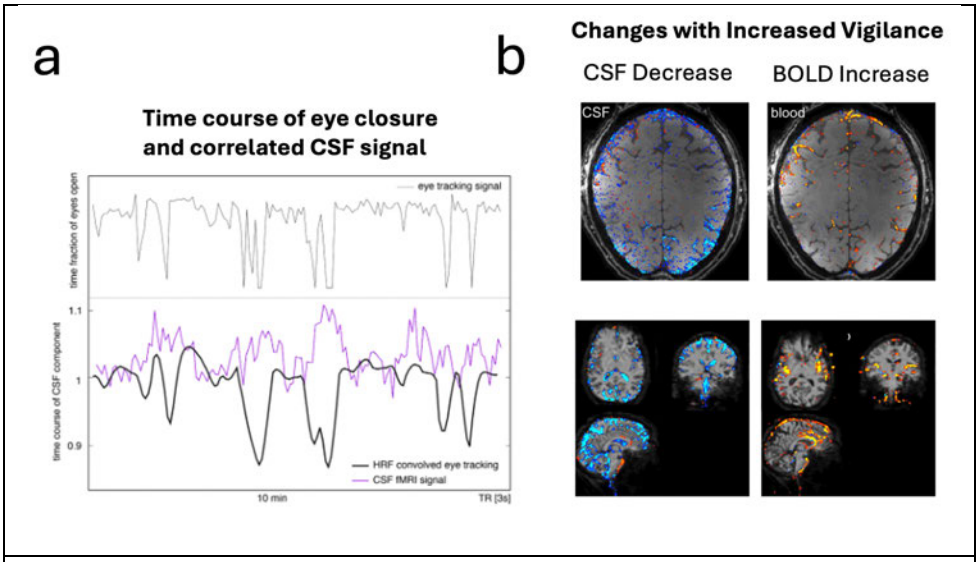


**Figure 19:** a) Time course of eye closure as measured with an eye tracker, showing discreet times where eyes were close over the course of a 10 minute scan. Here we show CSF volume increases in synchrony with the periods of eye closure or extreme drowsiness. Our model of the BOLD effect shows an opposite sign. Using these signals as regressors, we found that with increased vigilance, widespread CSF decreases and differently distributed BOLD increases are apparent.

We created a novel sequence that has the sensitivity, specificity, and speed to dynamically track functional changes of CSF, CBV, and BOLD concomitantly – opening up a new avenue for exploring neurofluid dynamics in the brain.

### 4.2 Functionally Time-Resolved Imaging

*A. Tyler Morgan, Isabel Gephart, Dan Handwerker, Javier Gonzalez-Castillo, Renzo Huber, Andy Derbyshire, Peter Bandettini*

High resolution fMRI (< 0.7 $mm^3$ voxels dimension) is essential for probing and mapping mesoscopic brain responses, yet tradeoffs in acquisition time and temporal stability are severe when imaging at ultra-high resolutions. High-resolution fMRI using EPI readouts and BOLD contrast suffer from spatial distortions and T2* blurring due to long readout trains. Here, we build on time resolved methods[24] to incorporate neuroscientific experimental designs and physiological confounds into fMRI reconstruction decisions to selectively bin k-space lines based on neuronal or physiologic events and therefore time resolve data from multi-echo, multi-shot gradient echo sequences, or more recently with EPI sequences – involving either one or very few k-space lines to minimize the readout time. Our method, functionally time-resolved fMRI (fTR), can image at very high spatial resolution (here, up to 0.5 mm) with multiple (six) echoes without sacrificing effective temporal resolution (here, 0.5 s). It is summarized in Figure 20.

Five subjects' data were collected on a Siemens MAGNETOM 7T+ w/ Nova 32Rx head coil. We collected two different sequences to demonstrate the utility of fTR-MRI: 1) a 2D GRE sequence (TR=31 ms, TEs=[4.22, 8.38, 12.54, 16.7, 20.86, 25.02] ms (bipolar readout), res=0.5x0.5 mm, slice thickness=0.8 mm, matrix=360x270, PE=R/L, repetitions=36, no acceleration or Partial Fourier, acquisition time=5:01). Prescription was perpendicular to the Calcarine Suclus. 2) a whole brain 3D GRE sequence (TR=4.5 ms, TE=2.1 ms, res=2.0 mm isotropic, FOV=216x220x88 mm, PE=A/P, repetitions=70).

Data were reconstructed via low-rank tensor completion with modes for k-space, receivers, echoes and response time. Initial k-space, channel and echo subspaces were derived using non-time resolved data with SVD. The time

subspace was either an informed 2-gamma HRF basis (with derivatives; experimental mapping), or an order-2 Fourier basis (physio mapping). The subspaces and rank-(20, 7, 3, 5) core tensor were then iteratively updated with available data until the 2-norm of the core converged. Participants were presented a flashing radial checkerboard (10 Hz; 2 s presentation, 15 s ISI) and were asked to fixate for the entire experiment. S0 & T2* maps were linearly fit to log-multi-echo data. These maps were used to segment gray matter of the calcarine sulcus region and to compute cortical depth values for each voxel (to plot layer-wise S0/T2* values) and 4 equi-volume layers (to plot response functions) using LAYNII software.

Functionally time-resolved fMRI incorporates experimental designs and physiology measures into image reconstruction to capture high spatial and temporal resolution brain responses. It also does not suffer from spatial distortions in the phase encoding direction, and the S0/T2* maps provide good anatomical contrast, aiding interpretation of experimental data. Future directions include combining task and physio mapping to better isolate task-related effects from layer fMRI responses.

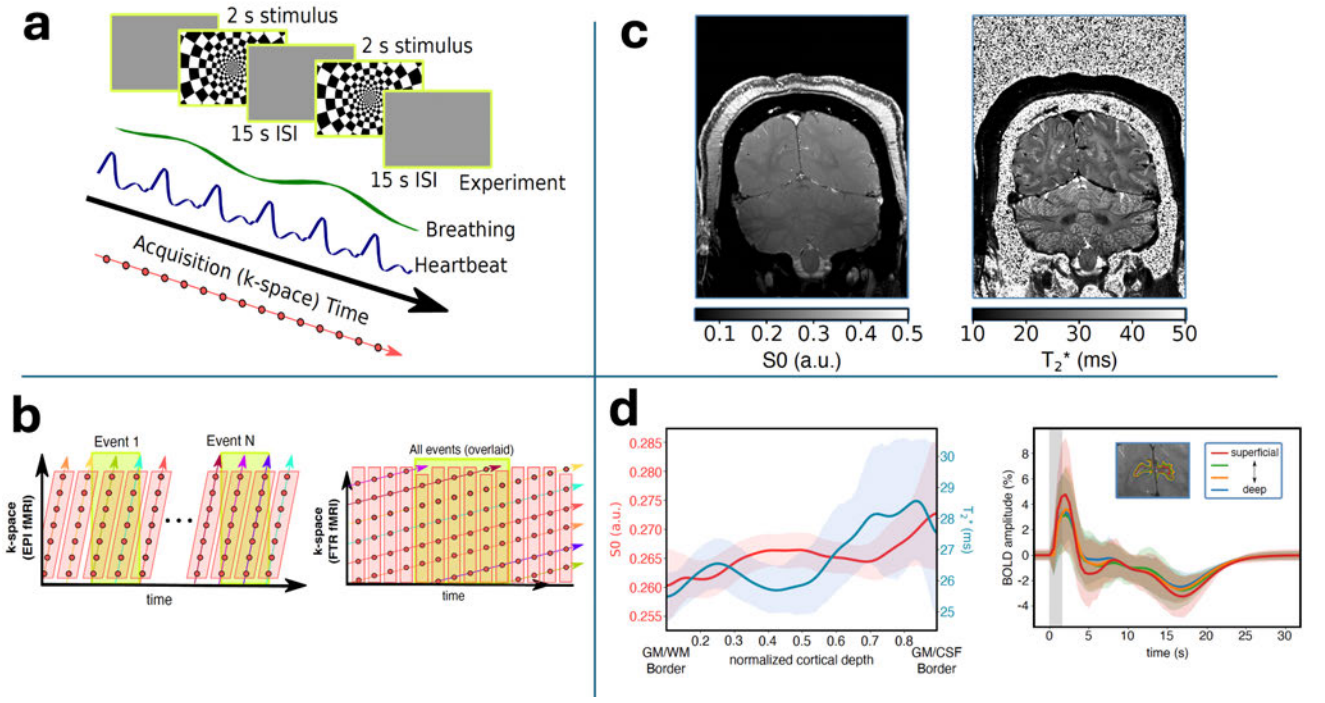


**Figure 20:** a) **Experimental and k-space acquisition timelines** are shown with concurrent physiologic processes affecting MRI image quality. b) In a typical fMRI experiment, k-space is sampled (colored arrows) as quickly as possible to form multiple images (red boxes) that form the time course. In functionally time-resolved (fTR) imaging, all experimental events are grouped and overlaid (green box) in order to fill k-space with a slower (but high-resolution) trajectory for specific images. The k-space data for each reconstructed image come from different times in the experiment, but reconstructed timelines are anchored to neuronal and physiological events of interest. c) **Reconstructed images.** Multi-echo data are used to fit high-resolution (0.5 mm) $S_0$ and T2* decay time parameters. Left: $S_0$ images display good gray/white matter and CSF contrast, enabling segmentation of functional data. Right: T2* images provide additional CSF and vascular contrast, as well as identification of striate cortex based on the visible Stria of Gennari. d) **Laminar analyses.** Left: Anatomical S0 and T2* values are plotted against normalized cortical depth values in the calcarine sulcus (see segmentation image on right). Shaded areas indicate 95% confidence intervals on the mean laminar profile. T2* display a characteristic dip in middle layers of striate cortex. Right: Functional BOLD responses (optimally combined echo data) to a 2-second flashing checkerboard stimulus (10 Hz) are shown for 4 cortical depth ROIs (see inset segmentation). The gray area indicates stimulation period, and shaded colors indicate 95% confidence intervals on individual voxel time courses. Superficial layers (red) show higher response amplitudes and larger undershoots than other cortical depths, similar to high-resolution temporal BOLD profiles seen in rodents.

## 4.3 Tedana: Leveraging Multi-Echo fMRI Analysis and Independent Regressors

*Daniel Handwerker, Eneko Urunuela, David Abbott, Peter Bandettini, Logan Dowdle, Marta Gomez, Javier Gonzalez-Castillo, Sarah Goodale, Neha Reddy, Robert Smith, Bahman Tahayori, Taylor Salo*

In 2012, a student in our lab, Prantik Kundu, figured out how to leverage multi-echo fMRI data to efficiently separate time series into those that follow echo time dependence (BOLD effects) and those that do not (artifact) by sorting the ICA components of the multi-echo time series based on their echo time dependence[25]. An international team convened and created a freely available tool called TE-dependent analysis (tedana)[26] that has helped catalyze the use of this powerful method of acquisition, resulting in multiple shared data sets *me-ica.github.io/open-multiecho-data/* as well as increase multi-echo implementation worldwide. SFIM members Daniel Handwerker and Joshua Teves helped to lead the development of tedana in two ways: 1. To increase ease of use and stability, and 2. To improve the effectiveness with which it denoises data.

In the past four years, we collaborated with the NIMH SSCC to integrate tedana with AFNI and to have processed data saved with appropriate Brain Imaging Data Structure (BIDS) specifications. We've aimed to make the processing steps of tedana more modular so that they may be independently modified or tested.

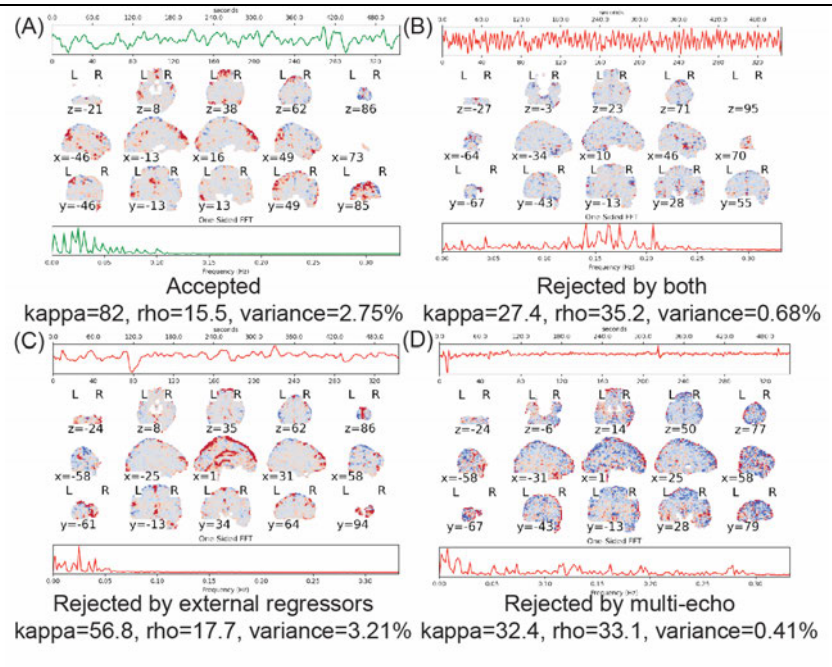


**Figure 21:** Four ICA components from a single run showing the series, the ICA weight map, and power spectrum below the map. A) Accepted. B) Rejected by both multi-echo and external regressor criteria (likely cardiac artifact) C) Rejected only by external regressors and might be a respiratory artifact with some BOLD weighting. D) Rejected only with multi-echo criteria (likely scanner artifact).

Recently, we've added the functionality of introducing external regressors such as head motion or respiration to query the ICA components. We've also enabled more straightforward adjustment of component parameters. An iterative Robust ICA[27] method was added. Quality control reporting now also includes measures that help identify more subtle variations in data.

To demonstrate the additional regressor fitting options and their benefit, we show, in Figure 21, tedana analysis of an audiovisual task where external nuisance regressors and multi-echo based denoising were independently compared. The value of this added feature is that artifactual signal, such as respiration, may show BOLD effects and therefore be missed by tedana but caught by an appropriate regressor, and vice versa for something perhaps like task correlated motion. By efficiently exploring these scenarios, the process of acquiring a deeper understanding of the signal and noise complexity is catalyzed, and the resulting functional images are further improved.

## Resources Requested

[redacted]

## Code, Data, and Resource Sharing

All lab members are now on **GitHub** and sharing their published data and code there, where it is linked to our website and accessible by a curated direct link: https://nimh-sfim.github.io/publications/ Data from several papers are also on **OpenNeuro**. Past shared data on the XNAT Central Data Repository is also being copied to **OpenNeuro**. It is worth noting that *all but 2 papers* that have an SFIM lead author from 2021-2024 that aren't reviews, opinion papers or book chapters, have shared data and/or code.

### Other data repositories than GitHub or OpenNeuro:

Chai, Y. et al. Neuroimage 2021, 242, 118455. **(OSF)**
Jangraw, D. C. et al. NeuroImage 2023, 282, 120390. **(OSF)**
Shahsavarani, S. et al. Cell Reports 2023, 42 (6). **(Zenodo)**

### Other Resources That Have been Shared:

**Tedana:** A publicly available collectively developed multi-echo analysis platform. This is described in section 4.3 above as well as in: *DuPre, E.; Salo, T.; Ahmed, Z.; Bandettini, P. A.; Bottenhorn, K. L.; Caballero-Gaudes, C.; Dowdle, L. T.; Gonzalez-Castillo, J.; Heunis, S.; Kundu, P.; Laird, A. R.; Markello, R.; Markiewicz, C. J.; Moia, S.; Staden, I.; Teves, J. B.; Urunuela, E.; Vaziri-Pashkam, M.; Whitaker, K.; Handwerker, D. A. TE-Dependent Analysis of Multi-Echo fMRI With Tedana. Journal of Open Source Software 2021, 6 (66), 3669.*

**rtPupilPhase:** Developed by Sharif Kronemer and colleagues for highly accurate real time detection of pupil phase. It is freely available and is described in section 3.2 above as well as in: *Kronemer, S. I.; Gobo, V. E.; Walsh, C. R.; Teves, J. B.; Burk, D. C.; Shahsavarani, S.; Gonzalez-Castillo, J.; Bandettini, P. A. Cross-Species Real-Time Detection of Trends in Pupil Size Fluctuation. Behavior Research Methods 2025, 57 (1), 1–14.*

**LayNii:** The development of this platform mostly happened elsewhere, however it is shared through methods that were developed in SFIM.

# Collaborations

| NIH | External Past SFIM/FMRIF Members | External |
|---|---|---|
| Alex Martin, Ph.D., NIMH, LBC<br>Eli Merriam, Ph.D., NIMH, LBC<br>Chris Baker, Ph.D., NIMH, LBC<br>Shruti Japee, Ph.D., NIMH, LBC<br>Laurentius Huber, Ph.D. NIMH FMRIF<br>Tyler Morgan, Ph.D., NIMH FMRIF<br>Linqing Li, Ph.D., NIMH FMRIF<br>Peter Molfese, Ph.D., NIMH FMRIF<br>Paul Taylor, Ph.D., and group, NIMH SSCC<br>Francisco Pereira, Ph.D., and group, NIMH MLT<br>Adam Thomas, Ph.D., and group, NIMH DSST<br>Maria Acosta, Ph.D., NHGRI<br>Misha Backonja, PhD., NCCIH<br>Diana Burk, Ph.D., NIMH | Yuhui Chai, Ph.D., Uof I at Urbana-Champaign<br>Elizabeth Wat, MD, Chldrn's Hosp. of Philadelphia<br>David Jangraw, Ph.D., University of Vermont<br>Isabel Gephart, University of Chicago<br>Emily Finn, PhD., Dartmouth College | Cesar Caballero Gaudes, Ph.D., BCBL, Spain<br>Elizabeth Hillman, Ph.D., and group, Columbia U<br>Max Riesenhuber, Ph.D., and group, Georgetown<br>Harri Piitulainen, Ph.D., University of Jyväskylä, FL<br>Tristan Bekinschtein, Ph.D., Cambridge, UK<br>Emily Jacobs, Ph.D., and group, UC Santa Barbara<br>Tom Liu, Ph.D., UC San Diego<br>Naomi Gaggi Ph.D., NYU, USA<br>Julia Kam, Ph.D., University of Calgary, CA<br>Benjamin Osborne, M.D., Georgetown<br>Tina Liu, Ph.D., Georgetown<br>Elizabeth DuPre, Ph.D., Stanford University<br>Taylor Salo, Ph.D., University of Pennsylvania<br>Logan Dowdle, Ph.D., Maastricht University<br>Stefano Moia, Ph.D., Maastricht University<br>Neha Reddy, Northwestern University, Chicago<br>Eneko Uruñuela, Ph.D., University of Calgary<br>David Abbott, Ph.D., and group, The Florey Institute of Neuroscience and Mental Health, University of Melbourne, Australia |

# COVID Statement

Our last BSC review in January 2021 took place in the midst of the COVID-19 pandemic. Like all labs around the world, LBC was impacted. Access to scanners, and even entry into the facilities, was not allowed between June 2020 and April 2021. Following this period, the return to work also took a bit of time due to additional government restrictions, only getting fully back to "normal" about 18 months ago. While an important aspect of our research was stalled, the crisis catalyzed new directions in research, and in particular, new analyses of large public datasets, which have been a productive avenue for research during this period.

# References


1. Chai, Y., Li, L., Huber, L., Poser, B. A. & Bandettini, P. A. Integrated VASO and perfusion contrast: A new tool for laminar functional MRI. *NeuroImage* **207**, 116358–116358 (2020).
2. Chai, Y. *et al.* Magnetization transfer weighted EPI facilitates cortical depth determination in native fMRI space. *NeuroImage* **242**, (2021).
3. Huber, L. (Renzo) *et al.* LayNii: A software suite for layer-fMRI. *NeuroImage* **237**, 118091 (2021).
4. Allan, T. W. *et al.* Functional Connectivity in MRI Is Driven by Spontaneous BOLD Events. *PLOS ONE* **10**, e0124577 (2015).
5. Esfahlani, F. Z. *et al.* High-amplitude cofluctuations in cortical activity drive functional connectivity. *Proc. Natl. Acad. Sci.* **117**, 28393–28401 (2020).
6. Ragone, E. *et al.* Modular subgraphs in large-scale connectomes underpin spontaneous co-fluctuation events in mouse and human brains. *Commun. Biol.* **7**, 1–14 (2024).
7. Liu, X. & Duyn, J. H. Time-varying functional network information extracted from brief instances of spontaneous brain activity. *Proc. Natl. Acad. Sci.* **110**, 4392–4397 (2013).
8. Betzel, R. F. *et al.* Hierarchical organization of spontaneous co-fluctuations in densely sampled individuals using fMRI. *Netw. Neurosci. Camb. Mass* **7**, 926–949 (2023).
9. Novelli, L. & Razi, A. A mathematical perspective on edge-centric brain functional connectivity. *Nat. Commun.* **13**, 2693 (2022).
10. Van Essen, D. C. *et al.* The WU-Minn Human Connectome Project: An overview. *NeuroImage* **80**, 62–79 (2013).
11. Schaefer, A. Local-global parcellation of the human cerebral cortex from intrinsic functional connectivity MRI. *Cereb Cortex* **28**, 1–20 (2017).
12. Margulies, D. S. *et al.* Situating the default-mode network along a principal gradient of macroscale cortical organization. *Proc. Natl. Acad. Sci.* **113**, 12574–12579 (2016).
13. Hasson, U., Nir, Y., Levy, I., Fuhrmann, G. & Malach, R. Intersubject Synchronization of Cortical Activity during Natural Vision. *Science* **303**, 1634–1640 (2004).

14. Eberhardt, L. V., Strauch, C., Hartmann, T. S. & Huckauf, A. Increasing pupil size is associated with improved detection performance in the periphery. *Atten. Percept. Psychophys.* **84**, 138–149 (2022).

15. Meissner, S. N. *et al.* Self-regulating arousal via pupil-based biofeedback. *Nat. Hum. Behav.* **8**, 43–62 (2024).

16. Ma, Y. *et al.* Resting-state hemodynamics are spatiotemporally coupled to synchronized and symmetric neural activity in excitatory neurons. *Proc. Natl. Acad. Sci.* **113**, E8463–E8471 (2016).

17. Shen, X. *et al.* Using connectome-based predictive modeling to predict individual behavior from brain connectivity. *Nat. Protoc.* **12**, 506–518 (2017).

18. Attarpour, A., Ward, J. & Chen, J. J. Vascular origins of low-frequency oscillations in the cerebrospinal fluid signal in resting-state fMRI: Interpretation using photoplethysmography. *Hum. Brain Mapp.* **42**, 2606–2622 (2021).

19. Chang, C. *et al.* Association between heart rate variability and fluctuations in resting-state functional connectivity. *NeuroImage* **68**, 93–104 (2013).

20. Tong, Y. *et al.* Evaluating the effects of systemic low frequency oscillations measured in the periphery on the independent component analysis results of resting state networks. *NeuroImage* **76**, 202–215 (2013).

21. Özbay, P. S. *et al.* Sympathetic activity contributes to the fMRI signal. *Commun. Biol.* **2**, 1–9 (2019).

22. Fultz, N. E. *et al.* Coupled electrophysiological, hemodynamic, and cerebrospinal fluid oscillations in human sleep. *Science* **366**, 628–631 (2019).

23. Kim, J.-H., Im, J.-G. & Park, S.-H. Measurement of CSF pulsation from EPI-based human fMRI. *NeuroImage* **257**, 119293 (2022).

24. Wang, F. *et al.* Echo planar time-resolved imaging (EPTI). *Magn. Reson. Med.* **81**, 3599–3615 (2019).

25. Kundu, P., Inati, S. J., Evans, J. W., Luh, W.-M. & Bandettini, P. A. Differentiating BOLD and non-BOLD signals in fMRI time series using multi-echo EPI. *Neuroimage* **60**, 1759–1770 (2012).

26. DuPre, E. *et al.* TE-dependent analysis of multi-echo fMRI with* tedana. *J. Open Source Softw.* **6**, 3669 (2021).

27. Anglada-Girotto, M., Miravet-Verde, S., Serrano, L. & Head, S. A. robustica: customizable robust independent component analysis. *BMC Bioinformatics* **23**, 519 (2022).